

**The Structure and Evolution of Lower Stratospheric Frontal Zones
Part I: Examples in Northwesterly and Southwesterly Flow**

By

ANDREA A. LANG and JONATHAN E. MARTIN

Department of Atmospheric and Oceanic Sciences
University of Wisconsin-Madison
1225 W. Dayton St.
Madison, WI 53706
(608) 262-9845
jemarti1@wisc.edu

Submitted for publication to *Quarterly Journal of the Royal Meteorological Society*
August 10, 2010

ABSTRACT

The structure, evolution, and dynamics of two lower stratospheric frontal zones are examined from a basic state variables perspective. The case studies highlight the asynchronous evolution of the lower stratospheric and upper tropospheric frontal portions of upper-level jet front (ULJF) systems, as well as some substantial differences in lower stratospheric frontal development that occur in southwesterly and northwesterly flow. The evolution of the ULJF in northwesterly flow was characterized by an initially intense but weakening lower stratospheric front along with an initially weak but intensifying upper tropospheric front. Throughout the evolution, geostrophic cold air advection in cyclonic shear characterized a substantial portion of the lower stratospheric front. This circumstance supported subsidence through the local jet core within the cold upper troposphere, weakening the lower stratospheric front via tilting. This subsidence extended downward below the jet core where it is suggested to have played a role in the early stages of upper tropospheric frontogenesis.

In the southwesterly flow case, the evolution of the ULJF was characterized by a strengthening lower stratospheric front and a weakening upper tropospheric front. A deep column of upward vertical motion resulted from the superposition of lower tropospheric ascent associated with convection along a surface cold front and upper tropospheric-lower stratospheric (UTLS) ascent through the jet core coincident with geostrophic warm air advection in cyclonic shear along large sections of the lower stratospheric front. The UTLS ascent, located on the cold edge of the lower stratospheric baroclinicity, served to intensify the lower stratospheric frontal zone via tilting. The implications of these lower stratospheric frontal processes on the energetics of ULJFs, the topography of the tropopause and downstream sensible weather are discussed.

1. Introduction

Upper level jet-front (ULJF) systems are ubiquitous dynamic and thermodynamic features found in the vicinity of the mid-latitude tropopause. These systems are characterized by a local wind speed maximum (i.e. the jet core) along the sloping mid-latitude tropopause surface. The regions of vertical shear located above and below the jet core are directly associated with attendant baroclinic zones (i.e. the fronts) via the thermal wind relationship (Figure 1). Since the mid 20th century, the structure, evolution, and life cycle of these ULJF systems have been studied in the context of clear air turbulence (e.g. Reed and Hardy, 1972; Kennedy and Shapiro, 1975, 1980, Shapiro, 1976; Keller, 1990), stratosphere-troposphere exchange and chemical transport (e.g. Danielsen, 1964; Shapiro, 1980; Holton et al., 1995; Stohl et al., 2003), and the extra-tropical cyclone life cycle (e.g. Uccellini et al., 1985; Sanders, 1988; Whitaker et al., 1988; Barnes and Colman, 1993; and Lackmann et al., 1997). For a detailed review of the first half-century of research on ULJFs the reader is directed to Keyser and Shapiro (1986).

To date, research into ULJFs has centered on the life cycle and associated implications of the upper tropospheric component of these systems, known as upper level fronts or upper tropospheric fronts (labeled “UT Front” in Figure 1). A number of studies, including Uccellini et al. (1985), Sanders (1988), Whitaker et al. (1988), Barnes and Colman (1993), and Lackmann et al. (1997), have demonstrated the role of upper tropospheric frontogenesis in the development of surface cyclones. These studies suggested that the ageostrophic transverse vertical circulation associated with a dynamically active ULJF not only provides the cross-stream differential subsidence required to intensify the upper level front, but simultaneously steepens and lowers the dynamic tropopause below the jet core. This process forces a thin wedge of stratospheric air,

characterized by large (small) values of potential vorticity (water vapor), downward into the upper and middle troposphere. Within the upper troposphere the large potential vorticity is manifest as a local maximum in absolute vorticity, providing an upper level precursor disturbance to a wave scale surface cyclogenesis event and implicating ULJFs in the incipient stages of the extra-tropical cyclone life cycle.

Additionally, the folding of the dynamic tropopause in association with intense upper tropospheric frontogenesis has been cited as one of the most efficient and dominant forms of stratosphere-troposphere exchange in the mid-latitudes (Mohanakumar, 2008). The role of individual ULJFs, specifically the upper tropospheric front, in stratosphere-troposphere exchange has been well documented (e.g. Danielsen, 1968; Shapiro et al., 1987; Lamarque and Hess, 1994; Eisel et al., 1999). The substantial displacements of the dynamic tropopause on isentropic surfaces that occurs within tropopause folds facilitate the exchange of mass across the tropopause (Stohl et al., 2003). As a result of the synoptic and mesoscale processes in the vicinity of a tropopause fold, dry, ozone-rich stratospheric air descends into the troposphere and can irreversibly mix with tropospheric air. It is hypothesized that at least 10% of global tropospheric ozone originates from the stratosphere via intense upper tropospheric frontogenesis and tropopause folding (Mohanakumar, 2008).

As deep, three-dimensional, features centered about the tropopause, ULJF systems have significant vorticity and thermal structures residing both in the upper troposphere *and* in the lower stratosphere (lower stratospheric front, labeled “LS Front” in Figure 1). While the majority of research attention regarding ULJFs has been focused on the upper tropospheric portions of these systems, little synoptic research attention has been given to the portions of these structures that reside above the jet core, within the lower stratosphere. The importance of the

lower stratospheric portion of mid-latitude ULJF systems has, for the most part, only been considered in so far as it is manifested in a zonally averaged sense and on seasonal timescales. As summarized by Shepherd (2002), the zonally averaged meridional temperature gradient, associated with the sloping mid-latitude tropopause, is coupled (via thermal-wind) to the zonal wind field at and above the tropopause. The zonal wind field there determines the propagation characteristics of atmospheric waves into the stratosphere, thus effecting the large scale stratospheric circulation and the seasonal scale stratosphere-troposphere exchange accomplished via the wave-driven Brewer-Dobson circulation. However, on shorter synoptic timescales the details of the structure, evolution, and dynamics of the lower stratospheric frontal portions of individual ULJF systems, remains incomplete. Similarly, the comprehensive role of ULJFs in the cyclone life cycle remains incomplete so long as the portions of ULJF systems that reside within the lower stratosphere continue to receive scant research attention. This paper will provide a contribution toward developing a more comprehensive view of the synoptic dynamics of the mid-latitude lower stratosphere by examining the structure, evolution, and dynamics of the lower stratospheric portions of two recently observed cases of ULJFs.

The paper is structured in the following manner: A history of research regarding the lower stratospheric portion of ULJFs and a background on frontogenesis is provided in section 2. A case study of ULJF evolution in northwesterly flow is presented in section 3. A case of ULJF evolution in southwesterly flow is presented in section 4. Finally, a summary and discussion of the analyses are provided in section 5.

2. Background

In one of the first conceptual models of an upper level jet-front system, Berggren (1952)

proposed that a continuous frontal zone (the polar front) stretched upward from the surface, through the upper troposphere and into the lower stratosphere (Figure 2). In the upper troposphere, the front was characterized by mesoscale gradients of temperature as well as cyclonic shear. At the level of maximum wind the feature was manifest solely as a mesoscale zone of cyclonic shear, while in the lower stratosphere, where the gradient of temperature reversed above the jet core, the front once again was characterized by both temperature gradients and cyclonic shear. This proposed model, which included mesoscale structures at and above the jet core, was largely dismissed due to lack of consistent balloon observation of the lower stratosphere (Palmén, 1958), allowing subsequent research attention to remain focused on the more consistently and conveniently observable upper tropospheric half of these systems. It was not until the 1960s, when instrumented research aircraft observations in field campaigns became a routinely available supplement to conventional radiosonde data, that a much improved resolution of ULJF structures was afforded (i.e. Danielsen, 1964; Shapiro, 1976). Using such high resolution aircraft measurements, Shapiro (1976) confirmed that there was indeed a mesoscale (~100 km) confinement of cyclonic wind shear below, at, and above the jet core. His analysis supported Berggren's hypothesis of a mesoscale frontal structure extending from the upper troposphere through the level of maximum wind, to the lower stratosphere. The regions of the ULJF that contained larger than background gradients of either potential temperature or cyclonic shear (or both) were termed “frontal” by Berggren (1952) and Shapiro (1976).

Though the notion of one continuous “frontal” region extending through the tropopause was thus suggested, theoretical and idealized studies (e.g. Eliassen, 1962; Shapiro, 1981) of ULJFs support the notion that two separate centers of frontogenetic forcing are vertically separated by the jet core. In fact, true fronts are regions characterized by both vertical *and*

horizontal shear as well as locally enhanced static stability (i.e. Newton and Trevisan, 1984; Hobbs et al., 1990; and Martin, 2006). Thus, the baroclinic zones in the upper troposphere and lower stratosphere can be characterized as two separate fronts, while the cyclonic shear region at the jet level, characterized as “frontal” by Berggren (1952) and Shapiro (1976), lacks the characteristics of a true frontal zone.

Early analyses of lower stratospheric thermal structure in the mid-latitudes revealed that above the jet core the warmest and coldest air were arranged in elongated parallel bands, horizontally separated by the wind speed maximum. This led several researchers (Riehl, 1948; Palmén, 1948; Palmén and Nagler, 1949) to hypothesize that the wind and thermal fields *above* the jet were connected with a cross-stream vertical circulation. These studies suggested that the vertical motions in the vicinity of the jet, by virtue of the strong static stability of the lower stratosphere, had a rather substantial effect on the horizontal thermal field via adiabatic warming and cooling. The investigations into the characteristics of the thermal structure above the jet core subsequently led to studies focusing on the nature of the vertical circulations in the vicinity of the jet. Palmén and Nagler (1949) originally proposed the idea that superimposed on the wave scale vertical motion between a ridge and downstream trough were two separate, cross-stream vertical circulations associated with the mid-latitude jet; one in the lower stratosphere above the jet core and another in the upper troposphere below the jet core. It was suggested that the upward and downward branches of these circulations, both in the upper troposphere and the lower stratosphere, could independently act to enhance or weaken the wave scale vertical motion associated with an upper-level trough. They suggested that the combination of the jet circulations and the wave scale vertical motions had a substantial effect on the production of sensible weather.

The pioneering work of Reed and Sanders (1953) and Reed (1955) established that differential vertical motions near the jet were at the heart of upper tropospheric frontal development. In the vicinity of the tropopause, the differential tilting of isentropes associated with cross-stream gradients of vertical motion could create sloping stable layers, with roots in the lower stratosphere, that were characterized by large horizontal temperature gradients. The differential vertical motion would also act to tilt horizontally oriented vortex tubes (associated with the vertical shear) into a more vertical orientation, thus enhancing the vertical vorticity within the developing upper level front.

In his extension of Sawyer's (1956) study on jet circulation dynamics, Eliassen (1962, his Figure 4) considered the forcing for two separate secondary circulation cells, one above and one below the jet core, associated with geostrophic deformation as described in the Sawyer (1956)-Eliassen (1962) equation. These two ageostrophic circulations were centered about the baroclinic zones lying above and below the level of maximum wind. A case analysis by Shapiro (1981) employed the Sawyer-Eliassen equation to calculate the geostrophic forcing and resulting ageostrophic secondary transverse circulations associated with a particularly intense ULJF. He illustrated that the geostrophic forcing above and below the jet are not necessarily equal (Shapiro 1981, his Figure 3c). In fact, his particular case depicted a scenario in which a larger geostrophic forcing was associated with the lower stratospheric front than with the upper tropospheric front. Despite the stronger geostrophic forcing in the lower stratosphere, Shapiro noted that the higher static stability in the lower stratosphere resulted in a weaker vertical circulation there than in the more weakly stratified upper troposphere. He consequently focused on the robust upper tropospheric development that characterized the case.

In a second analysis, Shapiro (1982) considered the secondary circulations associated

with idealized variations of the geostrophic shearing and stretching deformation forcings in the vicinity of the tropospheric half of the ULJF. He illustrated that in the absence of temperature advection (e.g. a case of pure stretching deformation), the Sawyer-Eliassen circulations in the jet entrance and exit regions resulted in the traditional four-quadrant model; a thermally direct (indirect) circulation in the entrance (exit) region (Figure 3a). In cases where cold air advection was present through the jet core, the thermally direct (indirect) circulation in the jet entrance (exit) region was shifted toward the anticyclonic (cyclonic) side of the jet, so that subsidence characterized the jet core (Figure 3b). Such a distribution of subsidence is consistent with that attributed to negative vorticity advection by the thermal wind (i.e. Sutcliffe, 1947; Trenberth, 1978), which exists along the jet axis when geostrophic cold air advection is present along an ULJF. Keyser and Pecnik (1987) showed that subsidence through the jet core is upper frontogenetic, thus the establishment of geostrophic cold air advection along the jet has been described as an important aspect of the upper front life cycle (Rotunno et al., 1994; Schultz and Doswell, 1999; Lang and Martin, 2010). An environment characterized by geostrophic warm air advection through the jet core shifts the thermally direct (indirect) circulation in the jet entrance (exit) region toward the cyclonic (anticyclonic) side, so that the jet core is conversely characterized by ascent (Figure 3c).

Figure 4 extends the Figure 3 conceptual model to the *stratospheric* half of an ULJF, where the geostrophic vertical shear and horizontal temperature gradient are reversed and illustrates the vertical motions forced by the idealized geostrophic stretching and shearing deformation *above the level of maximum winds*. An environment of pure geostrophic stretching deformation, illustrated as a straight jet streak in the absence of thermal advection, is shown in Fig 4a. Resembling the traditional tropospheric four-quadrant model, the thermally direct

entrance region and thermally indirect exit region are evident. However, in this lower stratospheric version of the four-quadrant model, the jet entrance (exit) region ascent is located on the cyclonic (anticyclonic) shear side of the jet, opposite to its location in the corresponding environment below the jet core. Figure 4b shows the resulting circulations forced by geostrophic cold air advection along an idealized jet. In this case, the thermally direct (indirect) circulation shifts toward the cyclonic (anticyclonic) shear side of the entrance (exit) region. Despite this altered distribution, the same outcome is produced in the lower stratosphere as in the upper troposphere, subsidence through the local jet maximum. Finally, the case of geostrophic warm air advection along the jet is illustrated in Figure 4c. As in the cold air advection case, though the entrance and exit region circulations shift in opposition to their counterparts below the jet core, the net result is a band of ascent through the local jet axis.

3. Northwesterly Flow Case

a. Synoptic Overview

During the first week of February 2008, an ULJF associated with the polar jet was situated in northwesterly flow over the west coast of the United States. As this ULJF rounded the base of an upper level trough between 4-5 February an intense upper tropospheric front developed. This upper tropospheric front was associated with the intensification of a mid-tropospheric shortwave that served as a precursor disturbance to a surface cyclogenesis event that brought several states in the Midwest upwards of 30 cm of snow on 5-6 February 2008. The focus of the present analysis is the northwesterly flow lower stratospheric frontal structure associated with the polar jet, prior to and during the early development of the upper tropospheric front. Using Eta-104 analyses, the evolution of the magnitude of the 200 hPa horizontal

potential temperature gradient will be used to represent the lower stratospheric front, as it was consistently located above the level of maximum winds of the northwesterly flow polar jet. The magnitude of the horizontal potential temperature gradient at 500 hPa will serve as a measure of the intensity of the upper tropospheric front. The magnitude of the potential temperature gradient within these two frontal structures affords a representation of the relative magnitude of available potential energy (APE) stored in both the lower stratospheric and upper tropospheric fronts.

At 0600 UTC on 4 February the 200 hPa flow was strongly baroclinic over the western United States (Figure 5a). Both the northwesterly and westerly flow around a broad trough were characterized by a long baroclinic zone, with a maximum magnitude of $\sim 8 \text{ K (100 km)}^{-1}$ slightly upstream of the trough axis, off the coast of California. The warmest potential temperatures at this level were located over the Great Basin, while the coldest potential temperatures were found in a region equatorward of and parallel to this main baroclinic zone. At 500 hPa, the upper tropospheric front associated with the polar jet was located in the same general area as its lower stratospheric counterpart, but its intensity was weaker, with a magnitude of only $\sim 6 \text{ K (100 km)}^{-1}$ over the California-Arizona border (Figure 5b).

By 1800 UTC 4 February, the amplitude of the 200 hPa trough had increased (Figure 6a). Off the coast of California, the lower stratospheric front was the noteworthy feature within the northwesterly flow with a magnitude that remained constant ($\sim 8 \text{ K (100 km)}^{-1}$). The magnitude of the thermal contrast decreased downstream of the trough axis. Though the amplification of the trough was notable at 200 hPa, at 500 hPa (Figure 6b) the baroclinicity associated with the upper tropospheric front actually weakened slightly as its maximum intensity dropped to $\sim 4 \text{ K (100 km)}^{-1}$. Clearly, through this time in the life cycle of this ULJF system, the upper

tropospheric front was much weaker than its robust lower stratospheric counterpart.

At 0600 UTC 5 February, the lower stratospheric front was oriented nearly north-south within the northwesterly flow, from Nevada to Baja California (Figure 7a). The maximum intensity of the lower stratospheric front had weakened slightly to $\sim 7 \text{ K (100 km)}^{-1}$ and it was centered over the California-Mexico border, upstream of the trough axis. The baroclinicity downstream, within the southwesterly flow, had nearly disappeared. While the lower stratospheric front began to weaken, the upper tropospheric front at 500 hPa became more coherent within the northwesterly flow immediately upstream of the trough axis, having strengthened to $\sim 6 \text{ K (100 km)}^{-1}$ while moving to northern Baja California (Figure 7b). At around this time a discernible shift in the relationship between these two frontal features was evident as the APE stored in the lower stratospheric front began to decrease while the APE within the upper tropospheric front increased.

By 1800 UTC 5 February, the amplitude of the 200 hPa trough had decreased (Fig 8a). Within the northwesterly flow, the roughly north-south oriented lower stratospheric front had further weakened in magnitude to $\sim 4 \text{ K (100 km)}^{-1}$ along the Arizona-Mexico border. Simultaneously, at 500 hPa, the upper tropospheric front continued to intensify, reaching a magnitude of $\sim 7 \text{ K (100 km)}^{-1}$ over the Big Bend region of Texas (Figure 8b). Continued strengthening of the upper tropospheric front (reaching a magnitude of $\sim 9 \text{ K (100 km)}^{-1}$ by 00 UTC 6 February, not shown) and erosion of the lower stratospheric part reinforced the growing disparity in APE that characterized these two features throughout the northwesterly flow portion of the ULJF system life cycle. Associated with the upper tropospheric development was the production of an upper level vorticity maximum (not shown) which acted as a precursor to surface cyclogenesis, a process described by Lackmann et al. (1997).

b. Analysis

The analysis focuses on 4 February, the period during the evolution of this ULJF in which the upper tropospheric front remained relatively weak while the lower stratospheric front was the dominant of the two frontal structures. Quasi-geostrophic (QG) forcing was used to diagnose regions of vertical motion in the vicinity of the polar jet's lower stratospheric (200 hPa) frontal zone. The full model vertical motion from the Eta-104 analyses, available every 6 hours, was used in calculations of tilting frontogenesis¹, $F_{g_{tilt}}$, where

$$F_{g_{tilt}} = -\frac{1}{|\nabla\theta|} \left[\frac{\partial\theta}{\partial p} \left(\frac{\partial\omega}{\partial x} \frac{\partial\theta}{\partial x} + \frac{\partial\omega}{\partial y} \frac{\partial\theta}{\partial y} \right) \right]. \quad (1)$$

At 0600 UTC 4 February, geostrophic cold air advection characterized the ULJF in the entrance region of the northwesterly jet at 200 hPa (Figure 9a). A maximum in geostrophic cold advection ($-12 \times 10^{-4} \text{ K s}^{-1}$) was located on the cyclonic shear side of the jet entrance region and in the vicinity of the most intense portion of the lower stratospheric front, just off the coast of central California. Coincident with this QG forcing for descent, subsidence was maximized (-8 cm s^{-1}) on the cold side of the lower stratospheric front and in the vicinity of the 200 hPa polar jet core (Figure 9b). As a consequence of this large region of subsidence, negative tilting frontogenesis ($\sim -32 \times 10^{-8} \text{ K m}^{-1} \text{ s}^{-1}$) characterized the majority of the northwesterly flow portion of the lower stratospheric front (Figure 9c) as sinking cold air acted frontolytically along the lower stratospheric front.

A vertical cross section taken through the polar jet along the line A-A' in Figure 9 is shown in Figure 10. The lower stratospheric and upper tropospheric fronts associated with the

¹ Tilting frontogenesis was calculated at 175 hPa as the vertical motion at this level was less “noisy” than at 200 hPa.

polar jet are apparent, though, the lower stratospheric front is the more intense of the two frontal features at this time (Figure 10a). The cyclonic shear side of this lower stratospheric front was also characterized by geostrophic cold air advection, with a maximum of $-18 \times 10^{-4} \text{ K s}^{-1}$ at ~ 275 hPa (Figure 10b). At ~ 230 hPa and within the largest wind speed at that level, there was a local maximum in subsidence (-10 cm s^{-1}) coinciding with the QG forcing along the lower stratospheric front. This subsidence was maximized above the jet core and to the cold side of the lower stratospheric front. Such subsidence decreased the slope of the isentropes and thus decreased the intensity and the APE of the lower stratospheric front above the jet core. The column of subsidence, most strongly forced in the lower stratosphere, extended downward through the weakly stratified jet core into the upper troposphere (Figure 10b) where it was maximized on the warm side of the upper tropospheric front and acted frontogenetically via tilting (not shown), an APE producing process.

By 1800 UTC 4 February, geostrophic cold air advection had intensified and characterized the majority of the northwesterly flow lower stratospheric frontal zone, from Oregon to off the west coast of northern Mexico (Figure 11a). The geostrophic cold air advection was generally confined to the cyclonic shear side of the geostrophic jet entrance region, with a maximum ($-21 \times 10^{-4} \text{ K s}^{-1}$) west of the California-Mexico border. The baroclinic zone associated with a subtropical jet crossing southern Baja California was also characterized by geostrophic cold air advection ($-12 \times 10^{-4} \text{ K s}^{-1}$). Subsidence was maximized (-10 cm s^{-1}) over northern Baja California, with a finger of locally larger values reaching upstream to the cold side of the lower stratospheric front. The gradient of vertical motion along the lower stratospheric front was associated with a linear band of negative tilting frontogenesis ($\sim -24 \times 10^{-8} \text{ K m}^{-1} \text{ s}^{-1}$), from the California-Oregon border south and east to the northern Gulf of California

(Figure 11c). Similar to the prior period, geostrophic cold air advection on the cyclonic shear side of the geostrophic jet entrance region was coincident with subsidence on the cold side of the lower stratospheric front. This subsidence acted frontolytically via tilting and acted to decrease the APE within the lower stratospheric front during period.

A second vertical cross section taken along the line B-B' in Figure 11 is shown in Figure 12. At this time, a majority of the lower stratospheric front above the jet core was characterized by geostrophic cold air advection in cyclonic shear. Geostrophic cold air advection stretched vertically from 350 hPa to 150 hPa and was maximized ($\sim -18 \times 10^{-4} \text{ K s}^{-1}$) at the 250 hPa level. Coincident with this forcing was a maximum in subsidence (-8 cm s^{-1}) at 250 hPa, within the local wind speed max and to the cold side of the lower stratospheric front. Subsidence on the cold side of the lower stratospheric front acted to decrease the slope of the isentropes above the jet core and continued to decrease the APE stored within the lower stratospheric front. Though this subsidence cannot be a result of QG processes associated with the upper tropospheric region of geostrophic warm air advection in cyclonic shear, it was located on the warm side of the weak upper tropospheric front and acted frontogenetically via tilting (not shown).

4. Southwesterly Flow Case

a. Synoptic Overview

Between 26-27 February 2008, a strong winter storm moved northeastward along the east coast of the United States (not shown). The cyclone prompted Winter Storm Warnings from North Carolina to Maine and left nearly 30 cm of snow in many areas of the Northeast. Further south, an intense squall line associated with an active trailing cold front brought severe

thunderstorms and power outages to the southeastern states. Temperatures in the wake of this cyclone were 15-20°F colder than normal for much of the East Coast. Using Eta-104 analyses, the deep baroclinic structure that developed within the upper troposphere and lower stratosphere in association with this cyclone will be investigated for the period between 27-28 February 2008.

At 0000 UTC 27 February, general southwesterly flow existed over the east coast of the United States (Fig 13). Within the southwesterly flow at 200 hPa, an enhanced baroclinic zone stretched from the southeast states toward Maritime Canada (Figure 13a). At this time, the lower stratospheric front had an intensity of $\sim 7 \text{ K (100 km)}^{-1}$ over the state of Maryland. The warmest temperatures at this level were found within the trough over the western Great Lakes region, while the coldest temperatures were found ahead of the lower stratospheric front, off the mid-Atlantic coast. At 500 hPa, the thermal structure was less coherent, with a weak upper tropospheric front over the southeastern states and weak regions of baroclinicity downstream (Figure 13b). The intensity of the upper tropospheric front was $\sim 5 \text{ K (100km)}^{-1}$ over the southern Appalachian Mountains. In the vicinity of the southeast states, the lower stratospheric and upper tropospheric fronts were generally parallel, however, at this particular time the lower stratospheric front was more intense than its tropospheric counterpart.

By 1200 UTC 27 February, the lower stratospheric front stretched from the Georgia-Florida border to Maritime Canada (Figure 14a). The maximum intensity of the lower stratospheric front remained constant ($\sim 7 \text{ K (100 km)}^{-1}$), however, the area characterized by such magnitude had grown substantially in the intervening 12-hours. A cold trough became more apparent immediately to the east of the lower stratospheric front, the upper troposphere-lower stratosphere equivalent of the thermal ridge ahead of a surface cold front. At 500 hPa, the most intense portion of the upper tropospheric front was found downstream of the confluence in the

flow, over the southeastern US (Figure 14b). The intensity of the potential temperature gradient associated with the upper tropospheric front had not changed since the previous time ($\sim 5 \text{ K (100 km)}^{-1}$). The upper tropospheric and lower stratospheric front were both fairly linear features, over the east coast of the US, with the lower stratospheric front being the more intense of the two fronts.

At 0000 UTC 28 February, the southwesterly flow over the east coast of North America was characterized by an intensifying lower stratospheric front (Figure 15a) with a maximum intensity of $\sim 8 \text{ K (100 km)}^{-1}$ over Maritime Canada. Immediately downstream of the 200 hPa trough axis, from the eastern Great Lakes northward into central Quebec, were the warmest potential temperatures at this level. Ahead of the lower stratospheric front, the thermal trough remained a robust feature, with the coldest temperatures just east of the most intense portion of the front. At 500 hPa, the upper tropospheric front weakened, with only two small regions in which $|\nabla\theta|$ was $\sim 5 \text{ K (100 km)}^{-1}$, over New Jersey and the South Carolina-Georgia border (Figure 15b). Over Maritime Canada, where the lower stratospheric front was at its most intense, the upper tropospheric front was nearly non-existent with a $|\nabla\theta|$ of $\sim 3 \text{ K (100 km)}^{-1}$.

By 1200 UTC 28 February, the lower stratospheric front stretched along the east coast of North America from the Bahamas to the region south of Greenland (Figure 16a). At 200 hPa, the region of intense baroclinicity ($|\nabla\theta| > \sim 6 \text{ K (100 km)}^{-1}$) characterized a larger area at this time and was flanked by the warmest potential temperatures ($\sim 369 \text{ K}$), over Newfoundland and the coldest potential temperatures ($\sim 330 \text{ K}$), over the northwestern Atlantic. In the upper troposphere, the southwesterly flow was characterized by a lengthy baroclinic zone with $|\nabla\theta| \sim 5 \text{ K (100 km)}^{-1}$ off the east coast of Maine. The upper tropospheric front stretched from the Carolinas to south of Greenland, however, the lower stratospheric front remained the more

intense of the two frontal features.

b. Analysis

The interaction of the constituent frontal zones of the ULJF on 28 February is examined next. This period represents the time when the lower stratospheric front was at its maximum intensity and covered the largest geographic area.

At 0000 UTC 28 February, southwesterly geostrophic flow was present along the east coast of North America, with a geostrophic jet max greater than 70 m s^{-1} off the southeast coast of the United States (Figure 17a). A majority of the cyclonic shear side of the southwesterly flow was characterized by geostrophic warm air advection, with a maximum in the jet exit region of $\sim 15 \times 10^{-4} \text{ K s}^{-1}$ east of New Jersey. Coincident with this geostrophic forcing, was a linear band of ascent on the cold side of the lower stratospheric front, over Florida and from east of the Carolinas to east of Newfoundland (Fig 17b). Ascent was greatest to the east and to the cold side of the maximum in geostrophic warm air advection. With ascent adiabatically cooling the cold side of the 200 hPa front, a nearly continuous band of positive tilting frontogenesis characterized the southwesterly flow lower stratospheric frontal zone from Florida to Newfoundland (Figure 17c). Several regions, including Florida, east of Maryland, and east of Newfoundland, had values of tilting frontogenesis greater than $20 \times 10^{-8} \text{ K m}^{-1} \text{ s}^{-1}$.

A cross section taken at 0000 UTC 28 February, perpendicular to the lower stratospheric front, along the line C-C' in Figure 17 is shown in Figure 18. Below the level of maximum winds, the tropospheric front was characterized by weak geostrophic cold air advection ($-6 \times 10^{-4} \text{ K s}^{-1}$). A plume of upward vertical motion was located immediately east of the surface cold front, was maximized at 500 hPa, and was associated with positive frontogenesis in the lower

troposphere (not shown). However, within the lower stratospheric front, a maximum ($15 \times 10^{-8} \text{ K m}^{-1} \text{ s}^{-1}$) in geostrophic warm air advection was present in the cyclonic shear centered at roughly 200 hPa. Immediately to the cold side of the lower stratospheric front and to the west of the lower tropospheric plume, was a second plume of ascent, with a maximum greater than 12 cm s^{-1} . Ascent in this location acted to increase the slope of the isentropes above the jet core (positive tilting frontogenesis) and acted to increase the slope of the tropopause above the jet core. The two plumes of vertical motion within this cross section were associated with two separate frontal circulations. One plume responded to frontogenetic forcing associated with the surface front in the lower troposphere while the other was coincident with QG forcing associated with the lower stratospheric front. Together these two plumes created a nearly vertically stacked column of ascent that reached from the surface to above the 150 hPa level, consuming APE in the troposphere and increasing the APE within the lower stratospheric front.

By 1200 UTC 28 February, the 200 hPa geostrophic jet had intensified to 80 m s^{-1} off the southeast coast of the United States (Figure 19a). Primarily downstream of the jet max, geostrophic warm air advection in cyclonic shear persisted through the majority of the southwesterly flow baroclinic zone. There were several maxima off the east coast of North America with values of geostrophic warm advection greater than $12 \times 10^{-4} \text{ K s}^{-1}$. In the vicinity of this QG forcing, a nearly continuous band of ascent characterized a large portion of the southwesterly flow, with the maximum roughly confined to the region of the jet core (Figure 19b). As a result, the tilting contribution to frontogenesis was positive and formed a roughly linear band from east of the Mid-Atlantic States to the region south of Greenland (Figure 19c).

A cross section was taken at 1200 UTC 28 February, along the line D-D' in Figure 19, through the straight southwesterly flow off the coast of Nova Scotia (Figure 20). The jet had

reached 90 m s^{-1} at roughly 250 hPa. Below the jet core, the broad, tropospheric-deep cold front was characterized by geostrophic cold air advection, with the greatest intensity ($-9 \times 10^{-4} \text{ K s}^{-1}$) located at ~ 450 hPa within the upper tropospheric portion of the front. This portion of the front was also characterized by subsidence. In the region above the jet core, geostrophic warm air advection characterized the cyclonic shear side of the jet and the lower stratospheric front. A large plume of ascent (10 cm s^{-1}), in the vicinity of the QG forcing in the lower stratosphere, was centered at roughly 225 hPa on the cold side of the lower stratospheric front. Ascent in the region continued to increase the slope of the isentropes above the jet core and tilt the dynamic tropopause into a more vertical orientation. By this time, the dynamic tropopause above the jet core had risen to ~ 150 hPa and the overall tropopause structure in the vicinity of the ULJF had become more steeply sloped.

5. Summary and Discussion

Upper-level jet front (ULJF) systems are ubiquitous features of the mid-latitude atmosphere consisting of an upper tropospheric frontal zone beneath the jet core, the jet core itself, and a lower stratospheric frontal zone above the jet core. Given their relevance to the extratropical cyclone life cycle, stratosphere/troposphere exchange, and clear air turbulence, the upper tropospheric portion of these ULJFs have been afforded considerable research attention in the past 60 years. Surprisingly little consideration has been given to the structure, evolution and dynamics associated with their lower stratospheric counterparts or the interaction between these separate frontal zones in the context of the ULJF life cycle. The present paper provides fresh insights into these issues by emphasizing the lower stratospheric front as a distinct entity within the ULJF and highlighting its structure, evolution, and dynamical interaction with its upper

tropospheric counterpart.

Consideration of the lower stratospheric portion of an ULJF as a distinct front encourages the extension of many of the concepts of upper tropospheric frontal dynamics to regions above the level of maximum wind. Analogous to Reed's (1955) description of an upper tropospheric front, the lower stratospheric baroclinic zone is best considered a frontal structure, with its own distinct frontal circulation, that separates stratospheric air from tropospheric air. Above the level of maximum winds, where the pole to equator temperature gradient reverses, the lower stratospheric front represents a boundary separating cold mid-latitude upper tropospheric air from warmer mid-latitude lower stratospheric air. Frontogenetic tilting across a lower stratospheric frontal zone will result from a combination of subsidence maximized in the warm lower stratosphere or ascent maximized in the cold upper troposphere, a thermally indirect circulation. Analogous to the situation in the upper troposphere, these differential vertical motions will result in the deformation of the tropopause above the level of maximum wind, where positive tilting frontogenesis is associated with a more steeply sloped tropopause. Based upon the examination of two cases, both observed in February 2008, the analysis presented here suggests that, though the governing dynamics for their developments (tilting frontogenesis) are the same, the upper tropospheric and lower stratospheric fronts develop asynchronously within the evolution of an ULJF through the northwesterly and southwesterly flow portions of a baroclinic wave.

In the northwesterly flow case, the ULJF was originally characterized by a vigorous lower stratospheric frontal zone and a weak upper-tropospheric frontal zone, as measured by the magnitude of the potential temperature gradients at 200 and 500 hPa, respectively. The lower stratospheric front was characterized by geostrophic cold air advection in cyclonic shear

(particularly in the jet entrance region) throughout the evolution. This circumstance was associated with subsidence on the cold side of the lower stratospheric frontal zone which, in turn, led to a decrease in its intensity. This subsidence, presumably forced by lower stratospheric frontal processes, protruded downward to sufficient depth to reach the warm side of the weak upper tropospheric front, gradually intensifying that feature. Thus, forcing for subsidence within the decaying lower stratospheric frontal environment is hypothesized to have been a contributing factor in an already favorable environment for the initial development of the upper tropospheric frontal portion of the ULJF. Furthermore, as the lower stratospheric front continued to weaken, the upper tropospheric front intensified demonstrating a clearly asynchronous, yet dynamically interactive developmental relationship between the two component frontal zones of the ULJF. The highlighted case is representative of several other cases analyzed in the course of this research. In each of these cases the northwesterly flow portion of a baroclinic wave is generally a region within which the lower stratospheric frontal zone of an ULJF experiences frontolysis while the upper tropospheric front experiences frontogenesis.

In the southwesterly flow case, the lower stratospheric front experienced a period of intensification coincident with the weakening of its upper tropospheric counterpart. In that case, the lower stratospheric front was characterized by a nearly continuous band of geostrophic warm air advection on the cyclonic shear side of the jet. Such a circumstance promotes QG forcing for ascent through the jet core, on the cold side of the lower stratospheric front. Such ascent was frontogenetic above the jet core increasing both the slope of the isentropes and the slope of the tropopause above the jet core. The ascent coincident with the lower stratospheric forcing was discernibly separate from the ascent associated with lower tropospheric frontal forcing. Their nearly vertical superposition, however, created a tropospheric deep column of ascent that acted

frontolytically in the middle and upper troposphere but frontogenetically in the lower stratosphere.

The results presented here appear to be characteristic of a number of other ULJF evolutions examined in the course of this research. To the extent that $|\nabla\theta|$ testifies to the amount of APE, the following conceptual model of the energetics of ULJF systems emerges from the research and is presented in schematic form in Figure 21. In northwesterly flow regimes, wherein the lower stratospheric frontal portion of the ULJF characteristically weakens while the upper tropospheric portion intensifies, it appears that APE is removed from the lower stratospheric front and invested in the upper tropospheric front (Figure 21). In southwesterly flow, wherein the lower stratospheric portion of the ULJF strengthens at the expense of the upper tropospheric frontal zone, it appears that APE is removed from the troposphere and invested in the lower stratosphere (Figure 21). In other words, the lower stratospheric frontal portion of the ULJF acts as a reservoir of APE that can be tapped in northwesterly flow (provided that cold air advection in cyclonic shear can be established) or replenished in southwesterly flow where thermally direct circulations in the troposphere are more commonly available to assist in increasing the slope of the tropopause above the jet core (e.g. through frontally forced or freely convective motions).

This study strongly suggests that consideration of the separate evolution of the lower stratospheric and upper tropospheric frontal zones associated with an ULJF system can lead to a better understanding of the comprehensive life-cycle of an ULJF through a baroclinic wave. It is left to future research to investigate how lower stratospheric frontal processes are explicitly connected to upstream or downstream sensible weather. For example, is lower stratospheric geostrophic warm air advection in cyclonic shear tied to ridge building and blocking in the way

that geostrophic cold air advection in the cyclonic shear within an upper tropospheric front is tied to upper level trough and cyclone development? Similarly, to the extent that lower stratospheric and lower tropospheric frontal circulations are vertically aligned, the kinetic energy released in any convective ascent along the tropospheric front can enhance the effect of the frontogenetic tilting already present in the lower stratospheric frontal circulation and thus further increase the APE being stored in an intensifying lower stratospheric front. The role that tropospheric convection plays in the intensification of the lower stratospheric thermal gradient in southwesterly flow cases remains an outstanding question.

The changes to the thermal field at and above the tropopause associated with lower stratospheric frontogenesis are also associated with variation in the structure of the vertical shear within the lower stratosphere. Thus, fully understanding lower stratospheric frontogenesis has further implications for the coupling between the stratosphere and troposphere by potentially explaining some of the variation in the environment governing the vertical propagation of atmospheric waves as the Sawyer-Eliassen forcing is the synoptic-scale version of the larger-scale Eliassen-Palm flux convergence. Perhaps consideration of lower stratospheric frontal processes will provide further insight into the not-yet-completely-understood role of synoptic scale baroclinic waves in transmitting the downward propagating anomalies, associated with the Northern Annular Mode (NAM), from the stratosphere to the troposphere (e.g. Baldwin and Dunkerton, 1999, 2001; Haynes, 2005; Breiteig, 2008).

REFERENCES

- Baldwin MP, Dunkerton TJ. 1999. Propagation of the Arctic Oscillation from the stratosphere to the troposphere. *J. Geophys. Res.* 104, 30937-30946.
- Baldwin MP, Dunkerton TJ. 2001. Stratospheric harbingers of anomalous weather regimes, *Science*, 294, 581-584.
- Barnes S, Colman B. 1993. Quasigeostrophic diagnosis of cyclogenesis associated with a cutoff extratropical cyclone - the Christmas 1987 storm. *Mon. Wea. Rev.* 121 (6) 1613-1634.
- Berggren R. 1952. The distribution of temperature and wind connected with active tropical air in the higher troposphere and some remarks concerning clear air turbulence at high altitude. *Tellus*, 4 43-54.
- Breiteig T. 2008. Extra-tropical synoptic cyclones and downward propagating anomalies in the Northern Annular Mode. *Geophys. Res. Lett.* 35 L07809.
- Danielsen EF. 1964. Project Springfield Report. Washington D. C., Defense Atomic Support Agency, DASA 1517, 97 pp. (DDC)
- Danielsen EF. 1968. Stratospheric-Tropospheric Exchange Based on Radioactivity, Ozone and Potential Vorticity. *J. Atmos. Sci.* 25, 3, 502-518
- Eisele H, Scheel HE, Sladkovic R, Trickl T. 1999. High-Resolution Lidar Measurements of Stratosphere-Troposphere Exchange. *J. Atmos. Sci.* 56, 2, 319-330
- Eliassen A. 1962. On the vertical circulation in frontal zones. *Geof. Publ.* 24 (4) 147-160.
- Haynes PJ. 2005. Stratospheric Dynamics. *Annu. Rev. Fluid Mech.* 37 263-293.

- Hobbs PV, Locatelli JD, Martin JE. 1990. Cold fronts aloft and the forecasting of precipitation and severe weather east of the rocky mountains. *Wea. Forecasting*. 5, 613-626.
- Holton JR, Haynes PH, McIntyre ME, Douglass AR, Rood RB, Pfister L. 1995. Stratosphere-Troposphere Exchange. *Rev. Geophys.* 33, 4. 403-439.
- Keller JL. 1990. Clear air turbulence as a response to meso- and synoptic-scale dynamic processes. *Mon. Wea. Rev.* 118, 2228–2242.
- Keyser D, Shapiro MA. 1986. A review of the structure and dynamics of upper level frontal zones. *Mon. Wea. Rev.* 114, 452-499.
- Keyser D, Pecneck MJ. 1985. A two-dimensional primitive equation model of frontogenesis forced by confluence and horizontal shear. *J. Atmos. Sci.* 42, 1259-1282.
- Kennedy PJ, Shapiro MA. 1975. The energy budget in a clear air turbulence zone as observed by aircraft. *Mon. Wea. Rev.* 103. 650-654
- Kennedy PJ, Shapiro MA. 1980. Further encounters with clear air turbulence in research aircraft. *J. Atmos. Sci.* 37, 986–993.
- Lackmann GM, Keyser D, Bosart LF. 1997. A characteristic life cycle of upper-tropospheric cyclongenetic precursors during Experiment on Rapidly Intensifying Cyclones over the Atlantic (ERICA). *Mon. Wea. Rev.*, 123, 1476-1504.
- Lamarque J-F, Hess PG. 1994. Cross-tropopause mass exchange and potential vorticity budget in a simulated tropopause folding. *J. Atmos. Sci.* 51, 15 pp. 2246–2269
- Lang AA, Martin JE. 2010. The influence of rotational frontogenesis and its associated shearwise vertical motions on the development of an upper level front. *Q. J. Roy. Meteor. Soc.*,

136, 239-252.

Martin JE. 2006. The role of shearwise and transverse quasigeostrophic vertical motions in the midlatitude cyclone life cycle. *Mon. Wea. Rev.* 134, 1174-1193.

Mohanakumar K. 2008. *Stratosphere-Troposphere Interactions: An introduction*. Springer, Heidelberg, Germany.

Newton CW, Trevisan A. 1984. Clinogenesis and Frontogenesis in Jet-Stream Waves. Part I: Analytical Relations to Wave Structure. *J. Atmos. Sci.* 41, 2717-2734.

Palmén E. 1948. On the distribution of temperature and wind in the westerlies. *J. Meteor.* 5, 20-27.

Palmén E, Nagler KM. 1949. Formation and structure of a large-scale disturbance in the westerlies. *J Meteor.* 6 (4) 227-242.

Palmén E. 1958. Vertical circulation and release of kinetic energy during the development of hurricane Hazel into an extratropical cyclone. *Tellus*, 10, 1-23.

Reed RJ. 1955. A study of a characteristic type of upper-level frontogenesis. *J. Meteor.*, 12, 226-237.

Reed RJ, Hardy KM. 1972. A case of persistent, intense, clear-air turbulence in an upper level frontal zone. *J. App. Metero.* 11, 541-549.

Reed RJ, Sanders F. 1953. An investigation of the development of a mid-tropospheric frontal zone and its associated vorticity field. *J. Meteor.*, 10, 338-349.

Riehl H. 1948. Jet stream in upper troposphere and cyclone formation. *Trans. Am. Geophys. Union*, 29, 175-186.

- Rotunno R, Skamarock WC, Snyder C. 1994. An analysis of frontogenesis in numerical simulations of baroclinic waves. *J. Atmos. Sci.*, **51**, 3373-3398.
- Sanders F. 1988. Life history of mobile troughs in upper westerlies. *Mon. Wea. Rev.* 116, 2629–2648.
- Sawyer JS. 1956. Dynamical aspects of some simple frontal models. *Q. J. R. Meteor. Soc.* 78 170
- Schultz DM, Doswell CA. 1999. Conceptual models of upper-level frontogenesis in southwesterly and northwesterly flow. *Quart. J. Roy. Meteor. Soc.*, 125, 2535-2562.
- Shapiro MA. 1976. The role of turbulent heat flux in the generation of potential vorticity in the vicinity of upper-level jet stream systems. *Mon. Wea. Rev.*, 104, 892–906.
- Shapiro MA. 1980. Turbulent mixing within tropopause folds as a mechanism of the exchange of constituents between the stratosphere and troposphere. *J. Atmos. Sci.* 37, 994-1004.
- Shapiro MA. 1981. Frontogenesis and geostrophically forced secondary circulations in the vicinity of jet stream-frontal zone systems. *J. Atmos. Sci.*, 38, 954–973.
- Shapiro MA. 1982. *Mesoscale Weather Systems of the Central United States*. CIRES Univ. of Colorado/NOAA, Boulder, Colo, USA. 78 pp.
- Shapiro MA, Hampel T, Krueger AJ. 1987. The arctic tropopause fold. *Mon. Wea. Rev.* 115,e 2, pp. 444–454
- Shepherd TG. 2002. Issues in stratosphere-troposphere coupling. *J. Meteorol. Soc. Japan.* 80, 769-792.
- Stohl A, Bonasoni P, Cristofanelli P, Collins W, Feichter J, Frank A, Forster C, Gerasopoulos E, Gäggeler H, James P, Kentarchos T, Kreipl S, Kromp-Kolb H, Krüger B, Land C,

- Meloan J, Papayannis A, Priller A, Seibert P, Sprenger M, Roelofs GJ, Scheel E, Schnabel C, Siegmund P, Tobler L, Trickl T, Wernli H, Wirth V, Zanis P, Zerefos C. 2003. Stratosphere-troposphere exchange - a review, and what we have learned from STACCATO. STACCATO special section of *J. Geophys. Res.* 108, 8516.
- Sutcliffe RC. 1947. A contribution to the problem of development. *Q. J. R. Meteorol. Soc.* 73. 370-383.
- Trenberth KE. 1978. On the interpretation of the diagnostic quasigeostrophic omega equation. *Mon. Wea. Rev.* 106, 131-137.
- Uccellini LW, Keyser D, Brill KF, Wash CH. 1985. The President's Day cyclone of 18-19 February 1979: Influence of upstream trough amplification and associated tropopause folding on rapid cyclogenesis. *Mon. Wea. Rev.* 113, 962-988.
- Whitaker JS, Uccellini LW, Brill KF. 1988. A model based diagnostic study of the Rapid development phase of the President's Day Cyclone. *Mon. Wea. Rev.* 116, 2337-2365.

Figure Captions

Figure 1. Vertical cross section of isotachs (m s^{-1} , solid) and isentropes (K, dashed) through an ULJF at 0000 UTC 17 April 1976, using NWS radiosonde data from Winslow, AZ (INW), Tuscon, AZ (TUS), and Fraccionamiento, Mexico (FRC) and supplemented with NCAR Sabreliner aircraft data. The regions of locally enhanced baroclinicity, static stability, and horizontal and vertical shear are shaded, representing the upper tropospheric front (UT Front) below the jet core and the lower stratospheric front (LS Front) above the jet core. Bold black line is the 1.5 PVU ($1 \text{ PVU} = 10^{-6} \text{ K m}^2 \text{ kg}^{-1} \text{ s}^{-1}$) identifying the dynamic tropopause. Adapted from Shapiro (1981).

Figure 2. Vertical cross section of isotachs (m s^{-1} , solid) and isentropes (K, dashed) from Valentia, Ireland to Hannover, Germany at 0300 UTC 9 November 1949. The shaded area represents a continuous frontal zone as described by Berggren (1952). Adapted from Berggren (1952).

Figure 3. Schematic illustration of idealized configurations of potential temperature along a straight jet streak maximum on an upper tropospheric isobaric surface. Geopotential height (thick solid), potential temperature (dashed), isotachs (thin solid filled) with the jet maximum represented by “J,” and a sense of the mid-tropospheric Sawyer-Eliassen vertical motions (up or down) for (a) no thermal advection along the jet (b) geostrophic cold air advection along the jet and (c) geostrophic warm air advection along the jet.

Figure 4. (a) – (c) As for Figure 3 (a) – (c) but for a lower stratospheric isobaric surface.

Figure 5. (a) 200 hPa geopotential height (solid), potential temperature (dashed), and magnitude of the horizontal potential temperature (shaded) from the Eta-104 model analysis valid at 0600 UTC 4 February 2008. Geopotential height is labeled in m and contoured every 200m, isentropes are labeled in K and contoured every 3 K, and the magnitude of the horizontal potential temperature gradient is shaded every $1 \text{ K (100 km)}^{-1}$ beginning at $2 \text{ K (100 km)}^{-1}$. (b) As for Figure 5(a) but at 500 hPa.

Figure 6. (a) and (b) As for Figure 5 (a) and (b), but from the Eta-104 model analysis valid at 1800 UTC 4 February 2008.

Figure 7. (a) and (b) As for Figure 5 (a) and (b), but from the Eta-104 model analysis valid at 0600 UTC 5 February 2008.

Figure 8. (a) and (b) As for Figure 5 (a) and (b), but from the Eta-104 model analysis valid at 1800 UTC 5 February 2008.

Figure 9. (a) 200 hPa geopotential height (thick solid), geostrophic isotachs (thin solid), isentropes (dashed), and geostrophic temperature advection (shaded) from the Eta-104 model analysis valid at 0600 UTC 4 February 2008. Geopotential height is contoured every 200 m, isentropes are labeled in K and contoured every 3 K, isotachs are labeled in m s^{-1} and contoured every 10 m s^{-1} , and dark (light) shading is geostrophic temperature advection contoured in units

of K s^{-1} every $-3 (3) \times 10^{-4} \text{ K s}^{-1}$. (b) Geopotential height (thick solid), isentropes (dashed), and vertical motion (shaded). Geopotential height is contoured as in Figure 9(a), isentropes are labeled and contoured as in Figure 9(a), and shaded solid (dashed) contours represent subsidence (ascent) and are contoured in cm s^{-1} every $-2 (2) \text{ cm s}^{-1}$ beginning at $-2 (2) \text{ cm s}^{-1}$. (c) Isentropes (dashed) and tilting frontogenesis (shaded). Isentropes are labeled and contoured as in Figure 9(a) and tilting frontogenesis is in units of $\text{K m}^{-1} \text{ s}^{-1}$ and contoured every $5 (-5) \times 10^{-9} \text{ K m}^{-1} \text{ s}^{-1}$ starting at $10 (-10) \times 10^{-9} \text{ K m}^{-1} \text{ s}^{-1}$ with dark (light) shading indicating negative (positive) tilting frontogenesis.

Figure 10. Vertical cross section along the line A-A' in Figure 9a valid at 0600 UTC 4 February 2008. (a) Potential temperature (thin solid), geostrophic isotachs (dashed), magnitude of the horizontal potential temperature gradient (shaded), and the tropopause (thick solid). Potential temperature is labeled in K and contoured every 4 K, isotachs are labeled in m s^{-1} and contoured every 10 m s^{-1} beginning at 30 m s^{-1} , the magnitude of the horizontal potential temperature gradient is contoured every 1 K (100km)^{-1} beginning at $2 \text{ K (100 km)}^{-1}$ and the tropopause is represented by the 1.5 PVU contour. (b) Potential temperature (thin light solid), isotachs (thin dark solid), geostrophic temperature advection (dashed), vertical motion (shaded), and the tropopause (thick solid). Potential temperature is labeled and contoured as in Figure 10(a), isotachs are labeled and contoured as in Figure 10(a), geostrophic temperature advection is contoured as in Figure 9(a) with dark (light) contours representing cold (warm) air advection, vertical motions are contoured as in Figure 9(b) with dark (light) shading representing subsidence (ascent), and the tropopause is represented as in Figure 10(a).

Figure 11. (a)-(c) As for Figure 9(a)-(c) but from the Eta-104 analysis valid 1800 UTC 4 February 2008.

Figure 12. As for Figure 10(b), but from the Eta-104 analysis valid 1800 UTC 4 February 2008 along the line B-B' in Figure 11(a).

Figure 13. (a) and (b) As for Figure 5 (a) and (b), but from the Eta-104 model analysis valid at 0000 UTC 27 February 2008.

Figure 14. (a) and (b) As for Figure 5 (a) and (b), but from the Eta-104 model analysis valid at 1200 UTC 27 February 2008.

Figure 15. (a) and (b) As for Figure 5 (a) and (b), but from the Eta-104 model analysis valid at 0000 UTC 28 February 2008.

Figure 16. (a) and (b) As for Figure 5 (a) and (b), but from the Eta-104 model analysis valid at 1200 UTC 28 February 2008.

Figure 17. (a)-(c) As for Figure 9(a)-(c) but from the Eta-104 analysis valid at 0000 UTC 28 February 2008.

Figure 18. As for Figure 10(b), but from the Eta-104 analysis valid at 0000 UTC 28 February 2008 along the line C-C' in Figure 17(a).

Figure 19. (a)-(c) As for Figure 9(a)-(c) but from the Eta-104 analysis valid at 1200 UTC 28 February 2008.

Figure 20. As for Figure 10(b), but from the Eta-104 analysis valid at 1200 UTC 28 February 2008 along the line D-D' in Figure 19(a).

Figure 21. Schematic illustrating the asynchronous evolution of the lower stratospheric (LSF) and upper tropospheric frontal (UTF) portions of an ULJF within the northwesterly and southwesterly flow portions of a baroclinic wave. The dashed shaded oval represents the northwesterly flow region where, within an ULJF, the lower stratospheric front experiences frontolysis via vertical tilting and the upper tropospheric front experiences frontogenesis via tilting. The solid shaded oval represents the southwesterly flow region where, within an ULJF, the lower stratospheric front experiences frontogenesis via vertical tilting and the upper tropospheric front experiences frontolysis via tilting. See text for additional explanation.

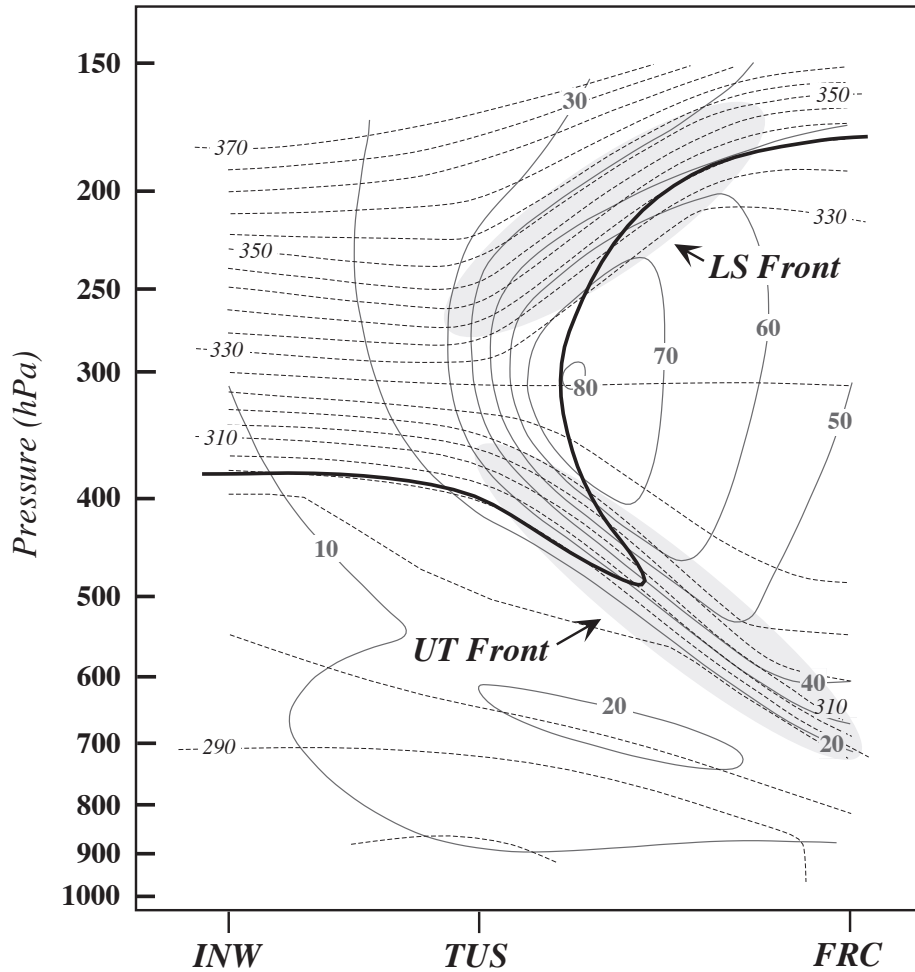


Figure 1. Vertical cross section of isotachs (m s^{-1} , solid) and isentropes (K, dashed) through an ULJF at 0000 UTC 17 April 1976, using NWS radiosonde data from Winslow, AZ (INW), Tucson, AZ (TUS), and Fraccionamiento, Mexico (FRC) and supplemented with NCAR Sabreliner aircraft data. The regions of locally enhanced baroclinicity, static stability, and horizontal and vertical shear are shaded, representing the upper tropospheric front (UT Front) below the jet core and the lower stratospheric front (LS Front) above the jet core. Bold black line is the 1.5 PVU ($1 \text{ PVU} = 10^{-6} \text{ K m}^2 \text{ kg}^{-1} \text{ s}^{-1}$) identifying the dynamic tropopause. Adapted from Shapiro (1981).

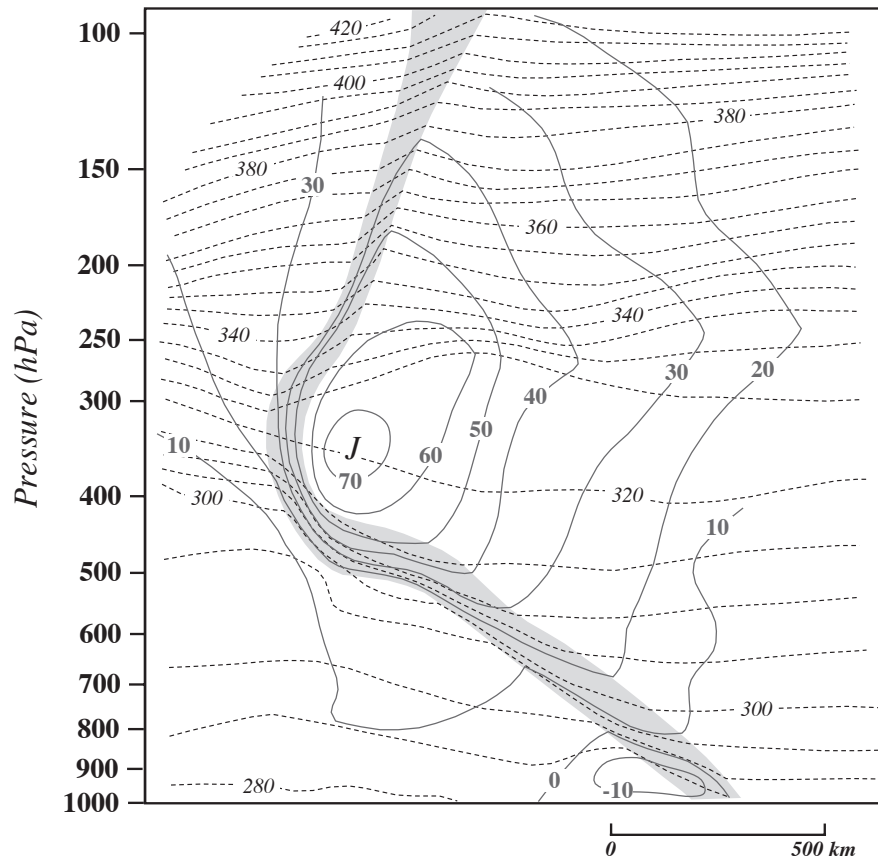


Figure 2. Vertical cross section of isotachs (m s⁻¹, solid) and isentropes (K, dashed) from Valentia, Ireland to Hannover, Germany at 0300 UTC 9 November 1949. The shaded area represents a continuous frontal zone as described by Berggren (1952). Adapted from Berggren (1952).

Upper Troposphere

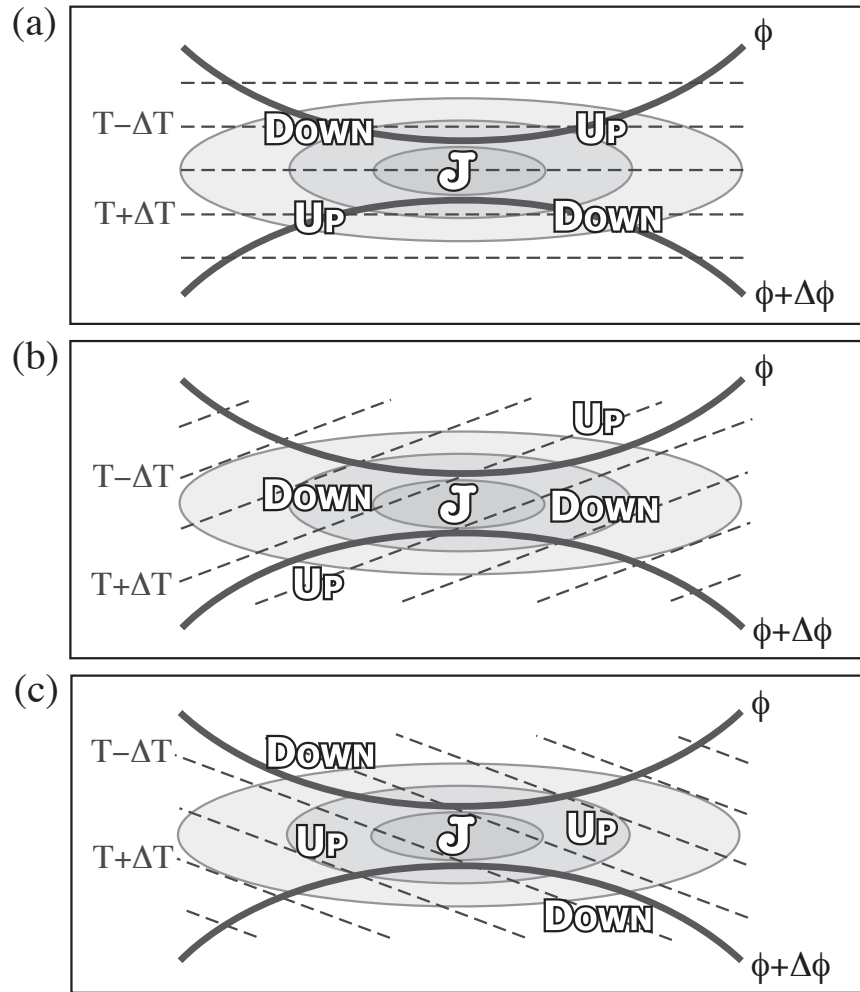


Figure 3. Schematic illustration of idealized configurations of potential temperature along a straight jet streak maximum on an upper tropospheric isobaric surface. Geopotential height (thick solid), potential temperature (dashed), isotachs (thin solid filled) with the jet maximum represented by “J,” and a sense of the mid-tropospheric Sawyer-Eliassen vertical motions (up or down) for (a) no thermal advection along the jet (b) geostrophic cold air advection along the jet and (c) geostrophic warm air advection along the jet.

Lower Stratosphere

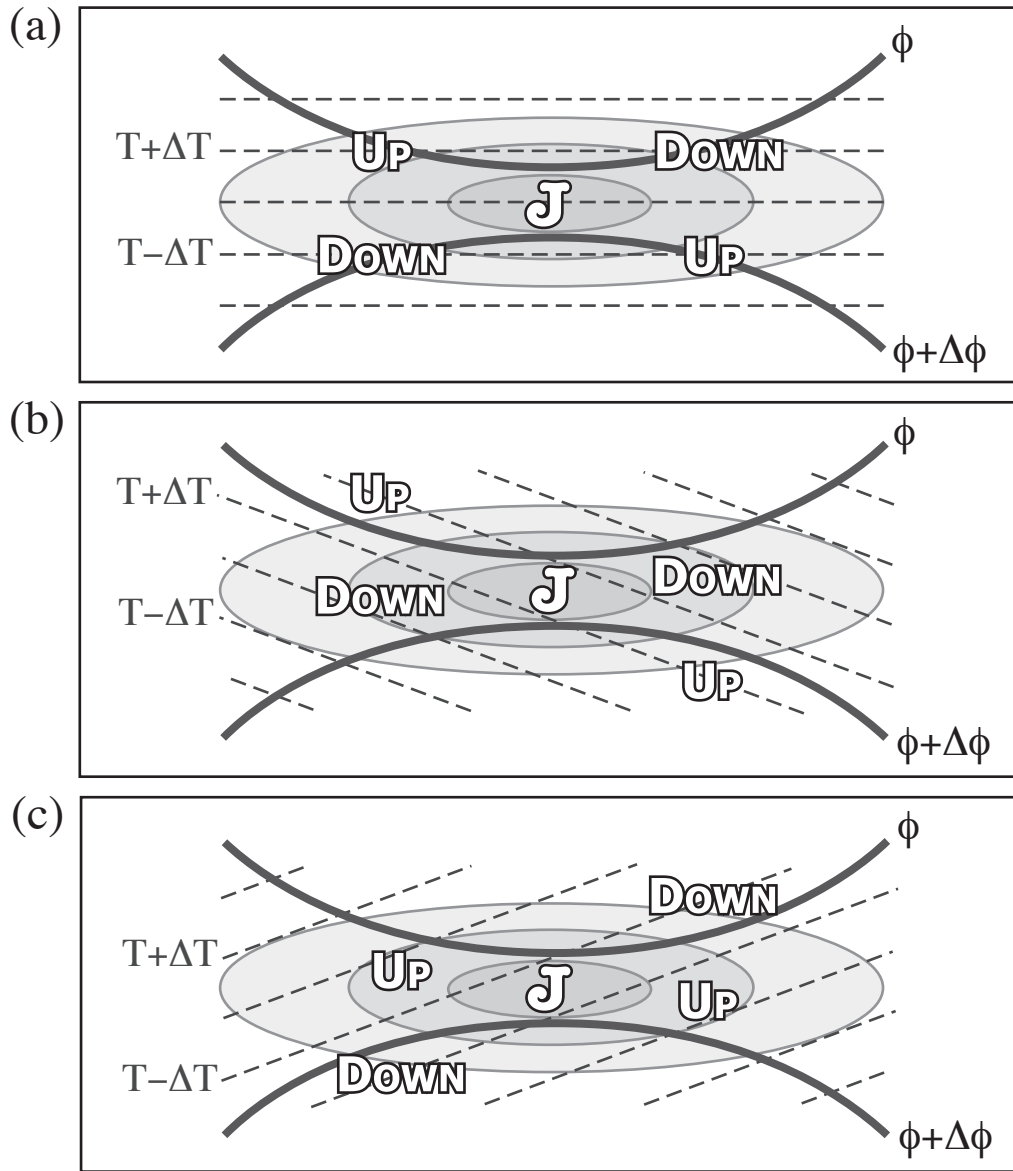


Figure 4. (a) - (c) As for Figure 3 (a) - (c) but for a lower stratospheric isobaric surface.

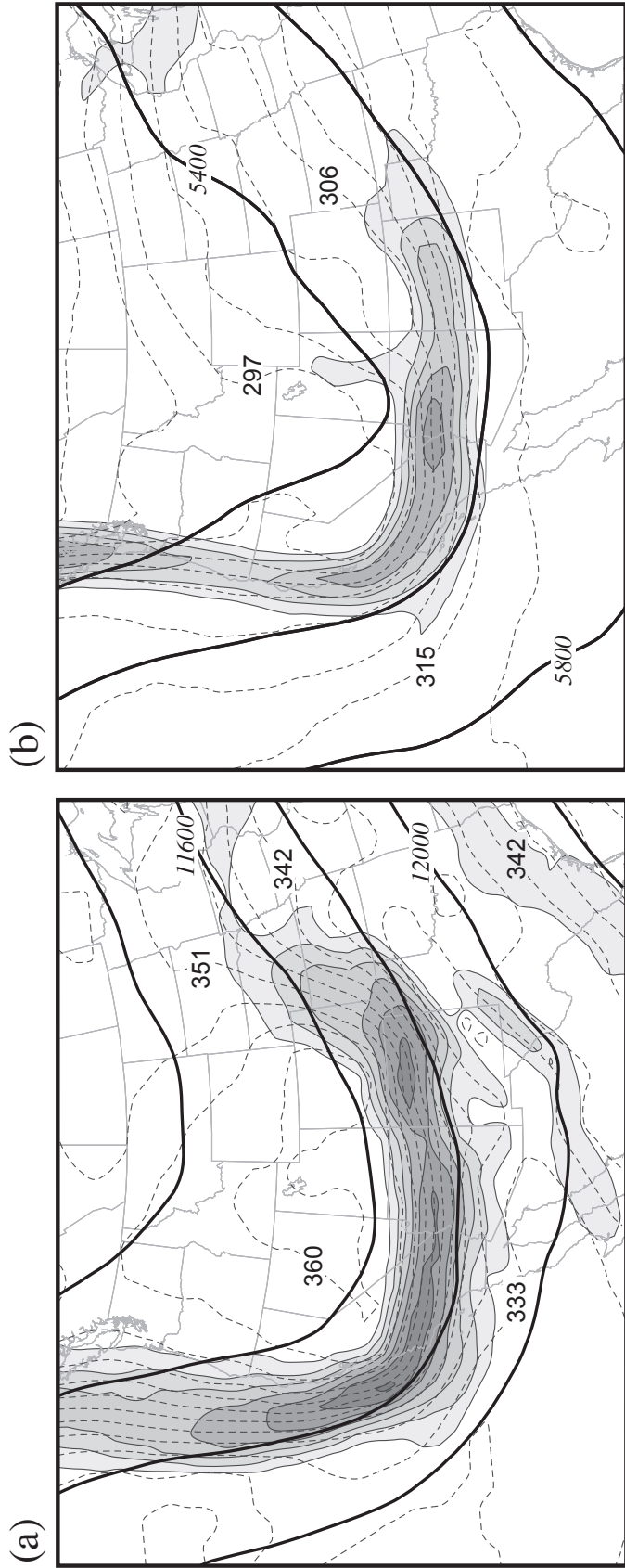


Figure 5. (a) 200 hPa geopotential height (solid), potential temperature (dashed), and magnitude of the horizontal potential temperature (shaded) from the Eta-104 model analysis valid at 0600 UTC 4 February 2008. Geopotential height is labeled in m and contoured every 200m, isentropes are labeled in K and contoured every 3 K, and the magnitude of the horizontal potential temperature gradient is shaded every 1 K (100 km)⁻¹ beginning at 2 K (100 km)⁻¹. (b) As for Figure 5(a) but at 500 hPa.

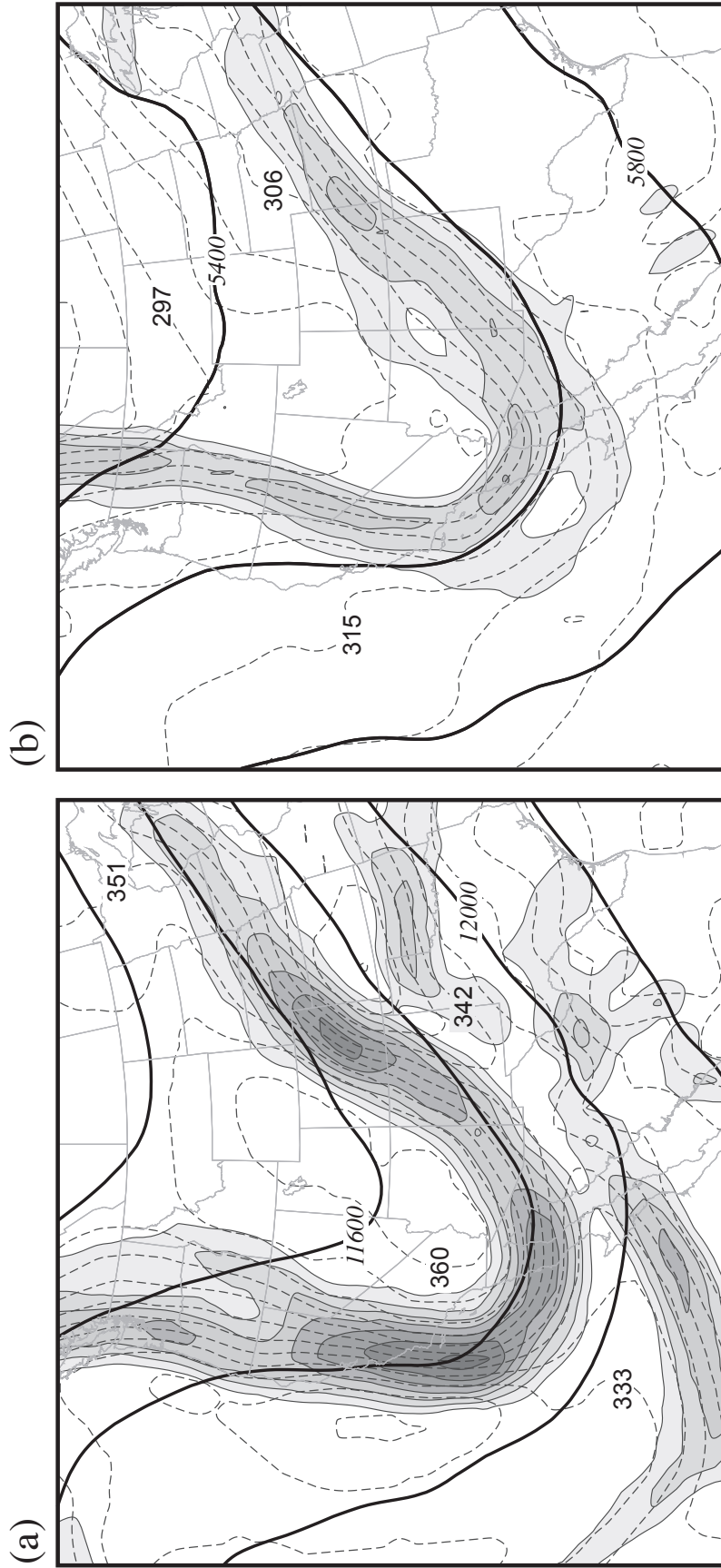


Figure 6. (a) and (b) As for Figure 5 (a) and (b), but from the Eta-104 model analysis valid at 1800 UTC 4 February 2008.

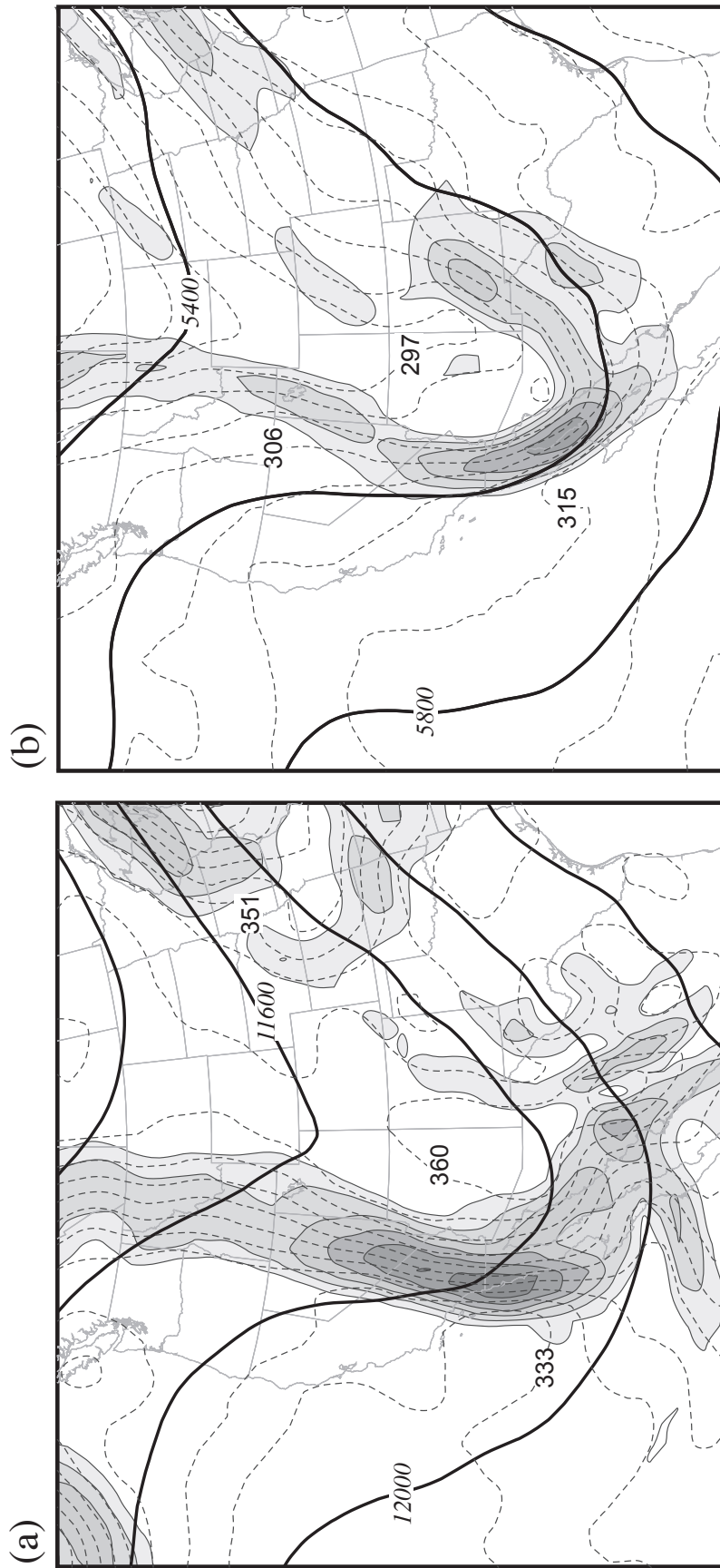


Figure 7. (a) and (b) As for Figure 5 (a) and (b), but from the Eta-104 model analysis valid at 0600 UTC 5 February 2008.

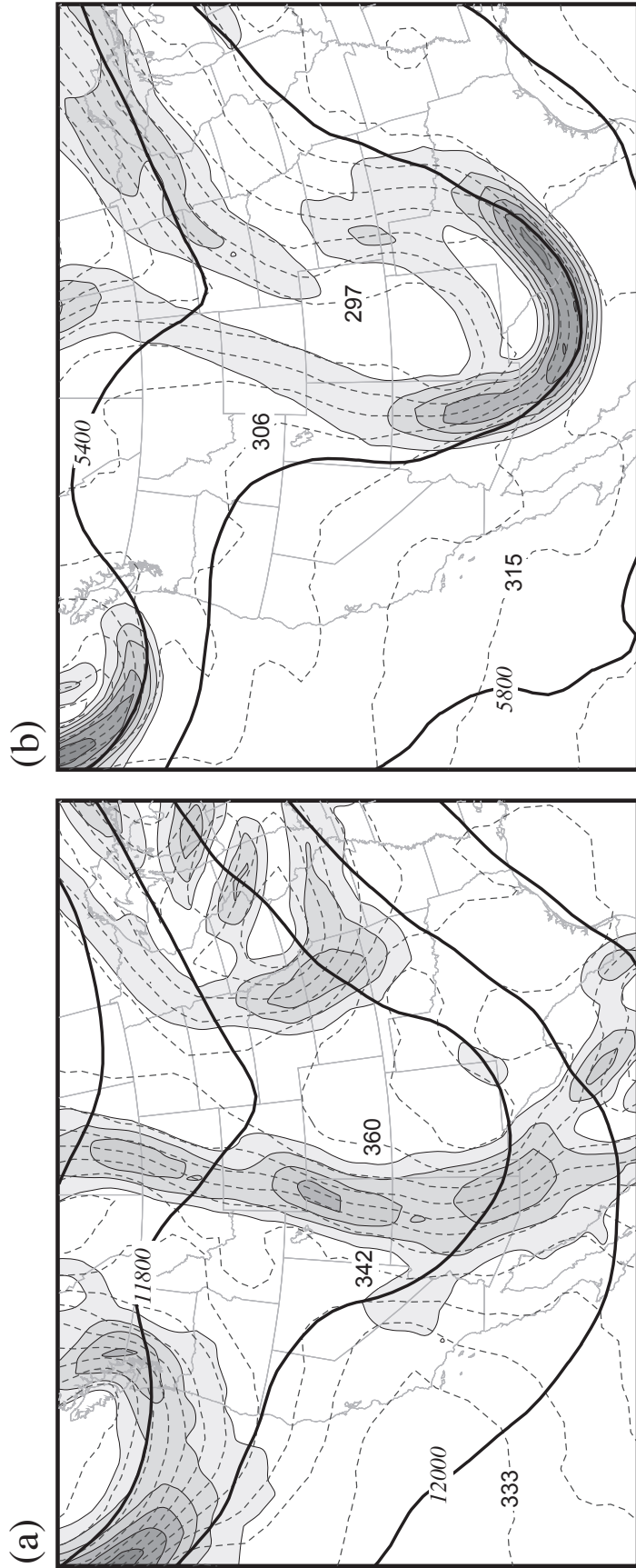


Figure 8. (a) and (b) As for Figure 5 (a) and (b), but from the Eta-104 model analysis valid at 1800 UTC 5 February 2008.

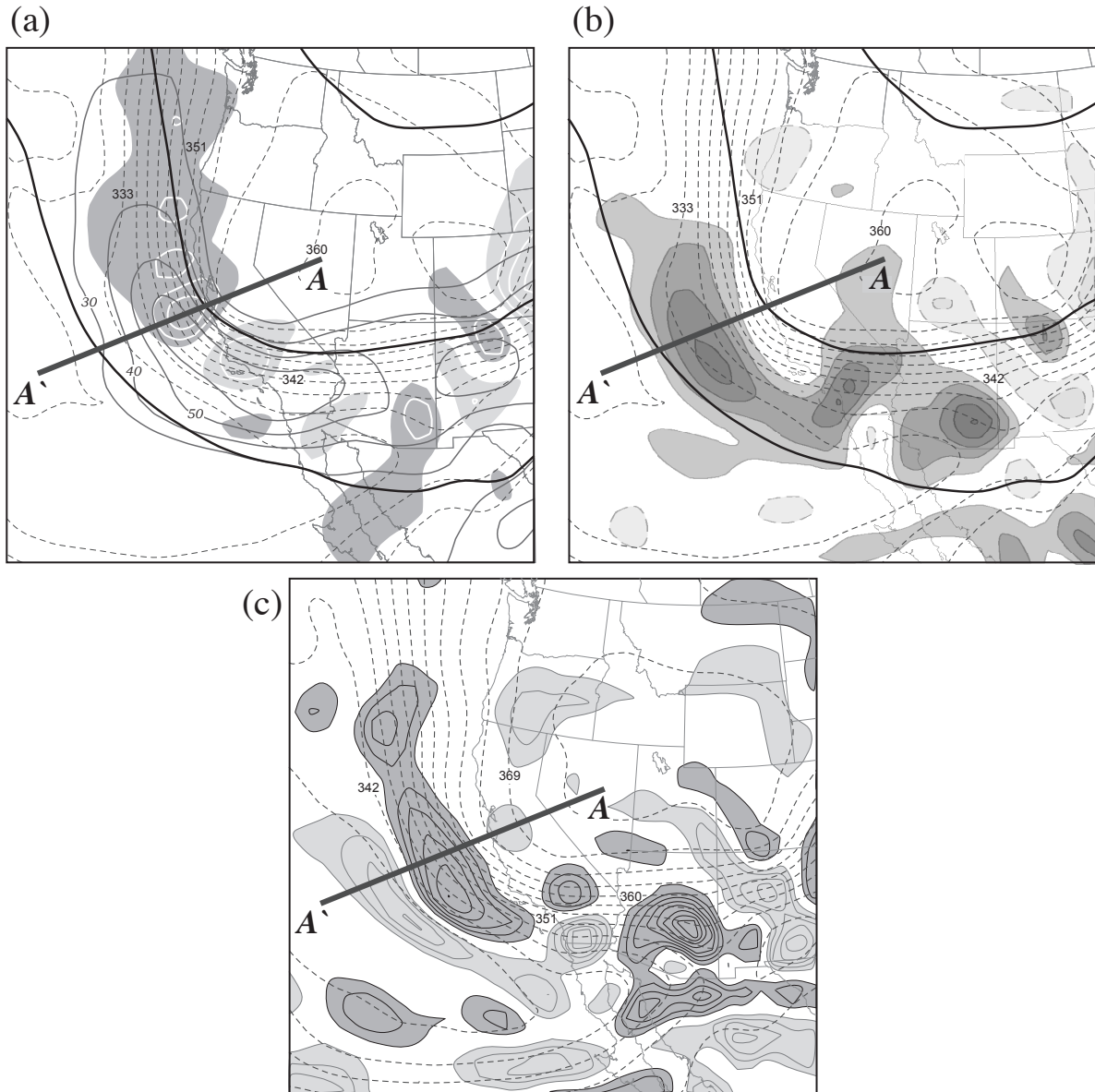


Figure 9. (a) 200 hPa geopotential height (thick solid), geostrophic isotachs (thin solid), isentropes (dashed), and geostrophic temperature advection (shaded) from the Eta-104 model analysis valid at 0600 UTC 4 February 2008. Geopotential height is contoured every 200 m, isentropes are labeled in K and contoured every 3 K, isotachs are labeled in m s^{-1} and contoured every 10 m s^{-1} , and dark (light) shading is geostrophic temperature advection contoured in units of K s^{-1} every $-3 (3) \times 10^{-4} \text{ K s}^{-1}$. (b) Geopotential height (thick solid), isentropes (dashed), and vertical motion (shaded). Geopotential height is contoured as in Figure 9(a), isentropes are labeled and contoured as in Figure 9(a), and shaded solid (dashed) contours represent subsidence (ascent) and are contoured in cm s^{-1} every $-2 (2) \text{ cm s}^{-1}$ beginning at $-2 (2) \text{ cm s}^{-1}$. (c) Isentropes (dashed) and tilting frontogenesis (shaded). Isentropes are labeled and contoured as in Figure 9(a) and tilting frontogenesis is in units of $\text{K m}^{-1} \text{ s}^{-1}$ and contoured every $5 (-5) \times 10^{-9} \text{ K m}^{-1} \text{ s}^{-1}$ starting at $10 (-10) \times 10^{-9} \text{ K m}^{-1} \text{ s}^{-1}$ with dark (light) shading indicating negative (positive) tilting frontogenesis.

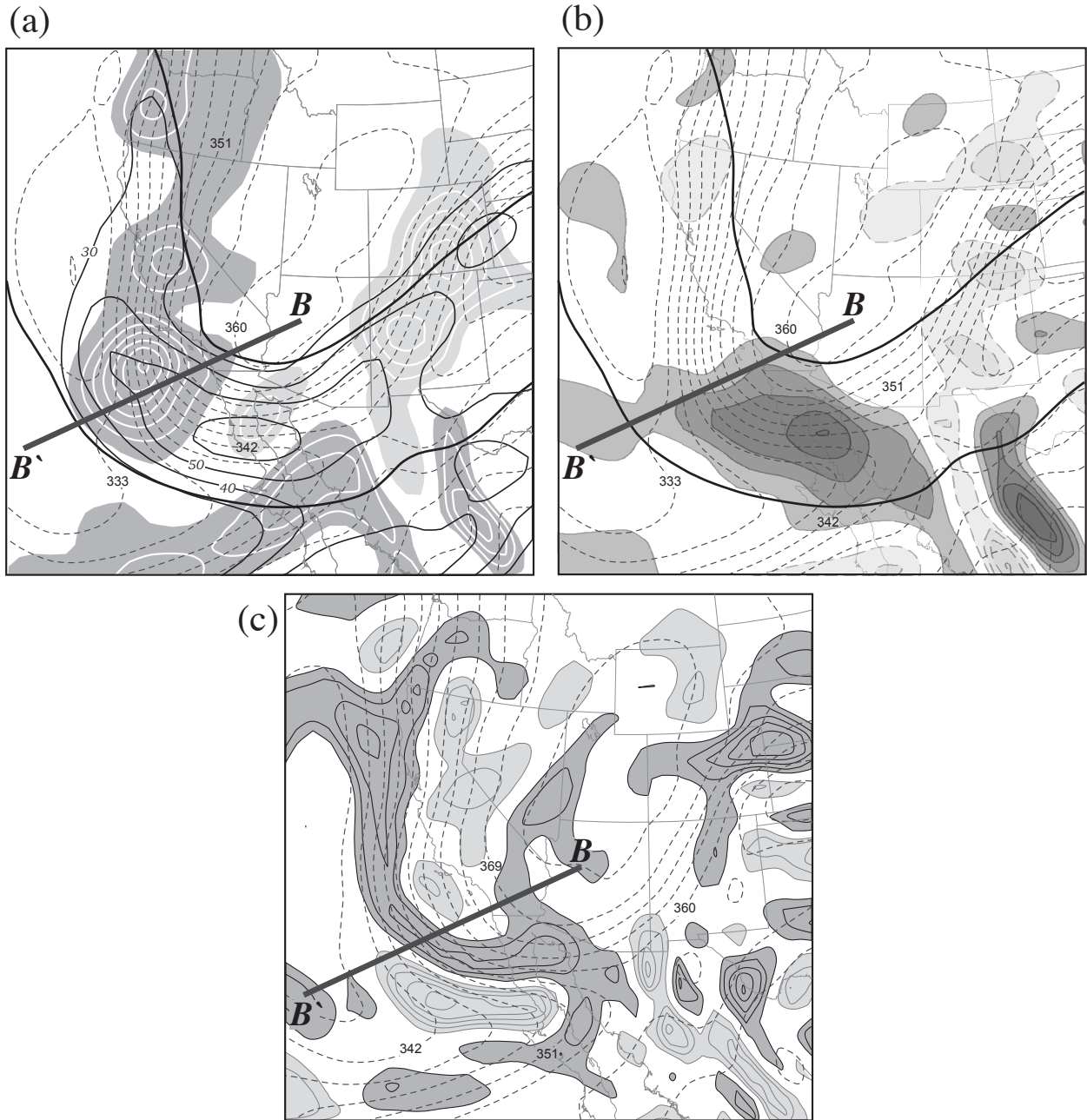


Figure 11. (a)-(c) As for Figure 9(a)-(c) but from the Eta-104 analysis valid 1800 UTC 4 February 2008.

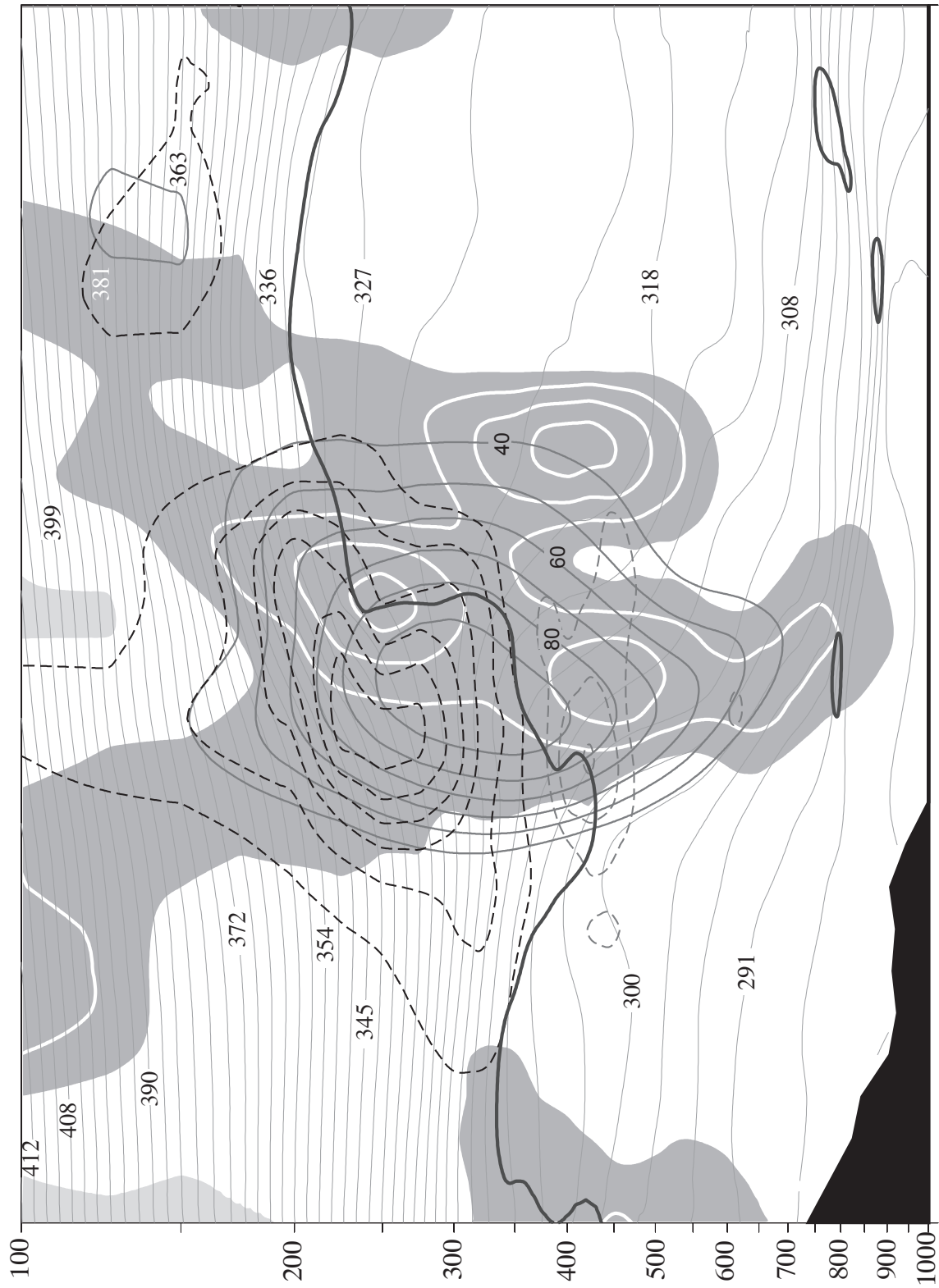


Figure 12. As for Figure 10(b), but from the Eta-104 analysis valid 1800 UTC 4 February 2008 along the line B-B' in Figure 11(a).

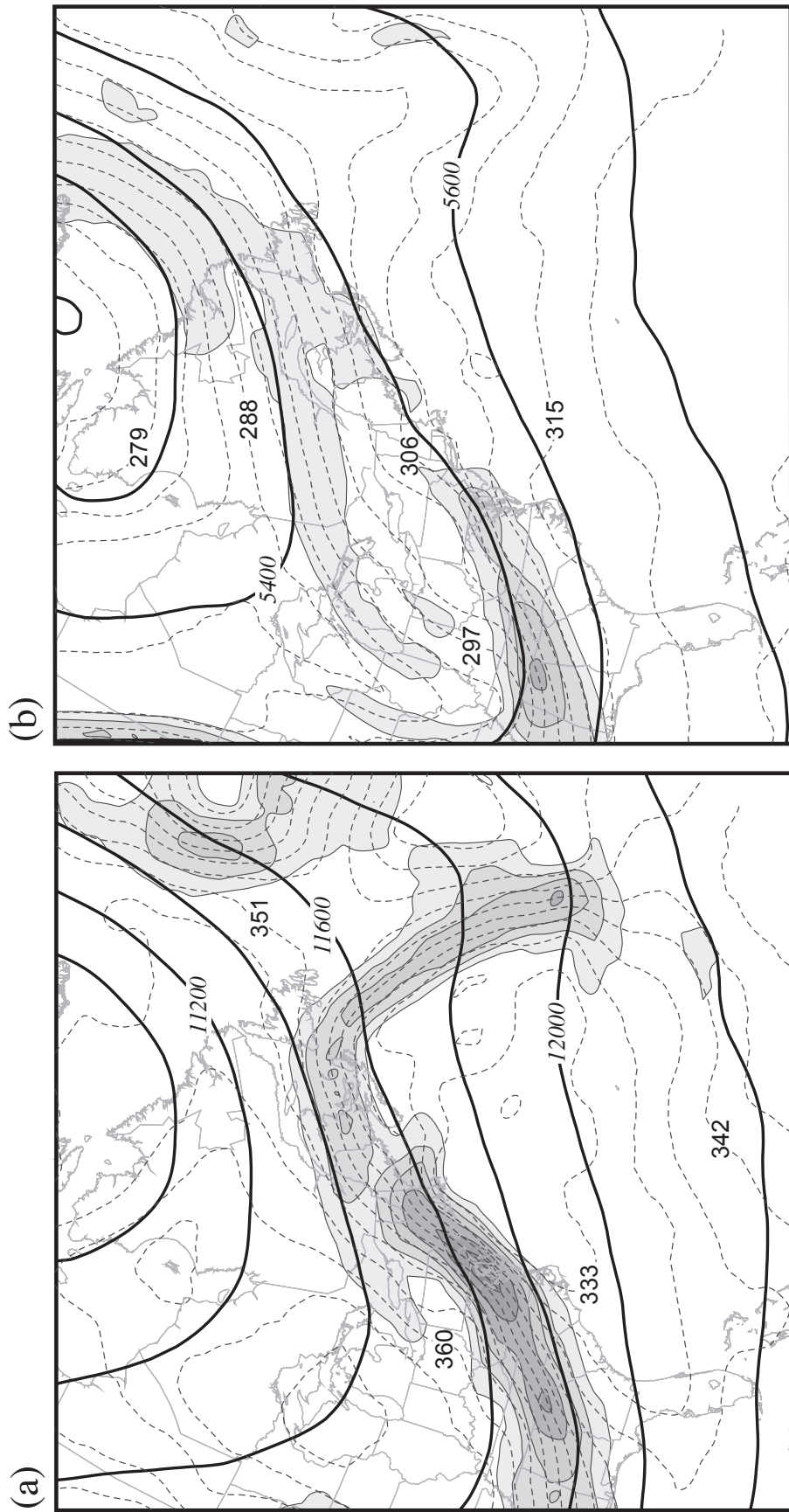


Figure 13. (a) and (b) As for Figure 5 (a) and (b), but from the Eta-104 model analysis valid at 0000 UTC 27 February 2008.

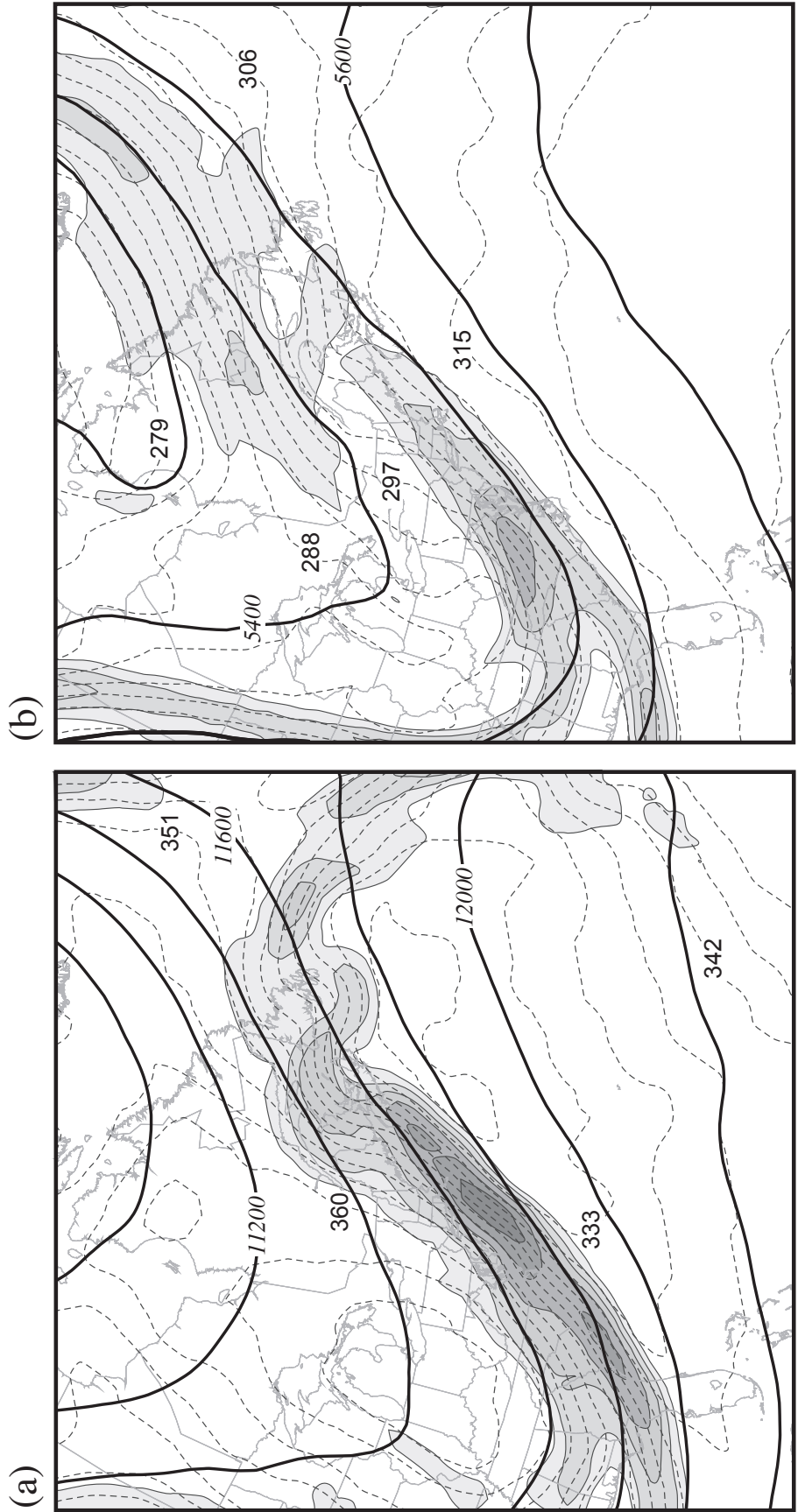


Figure 14. (a) and (b) As for Figure 5 (a) and (b), but from the Eta-104 model analysis valid at 1200 UTC 27 February 2008.

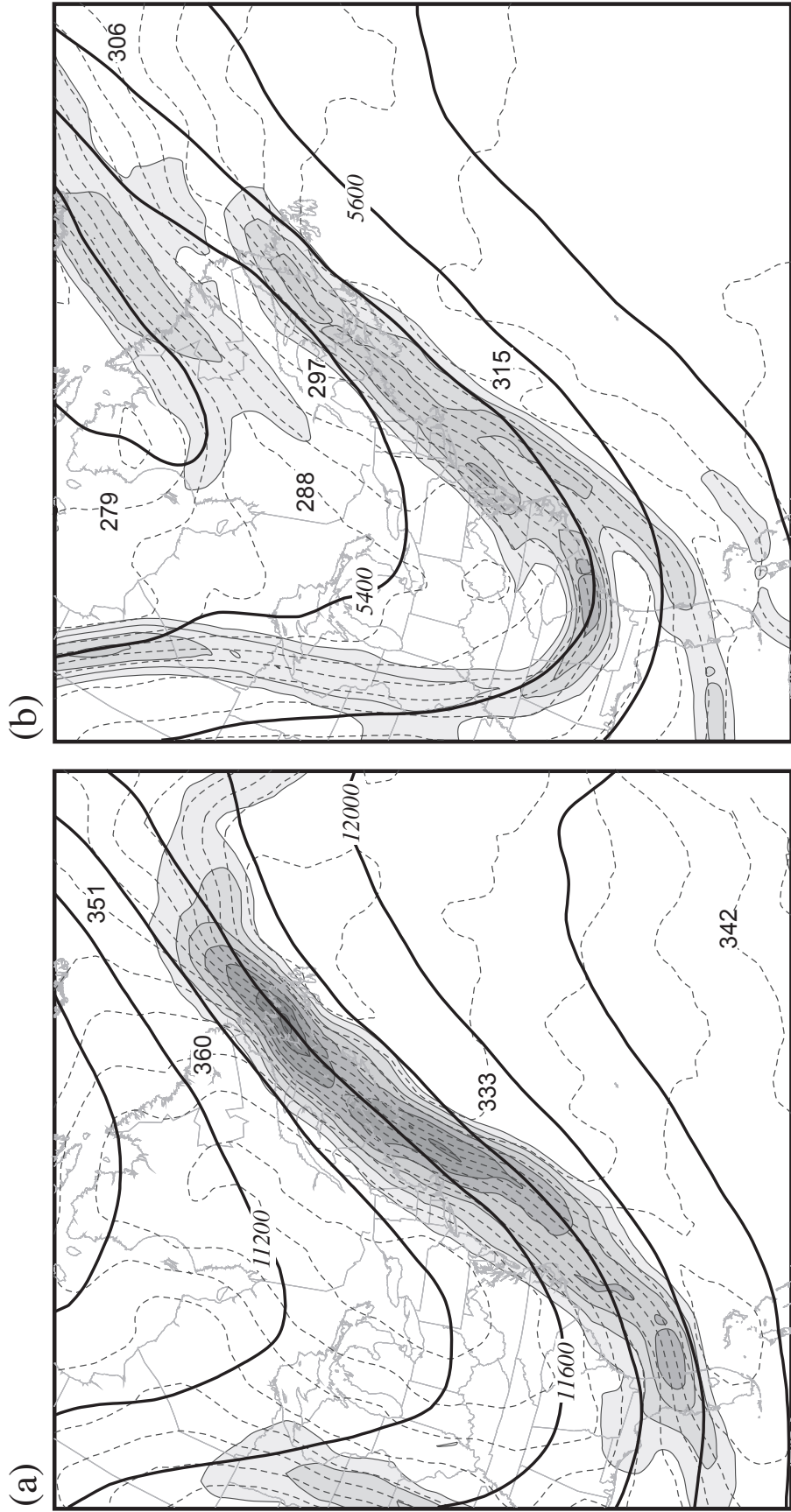


Figure 15. (a) and (b) As for Figure 5 (a) and (b), but from the Eta-104 model analysis valid at 0000 UTC 28 February 2008.

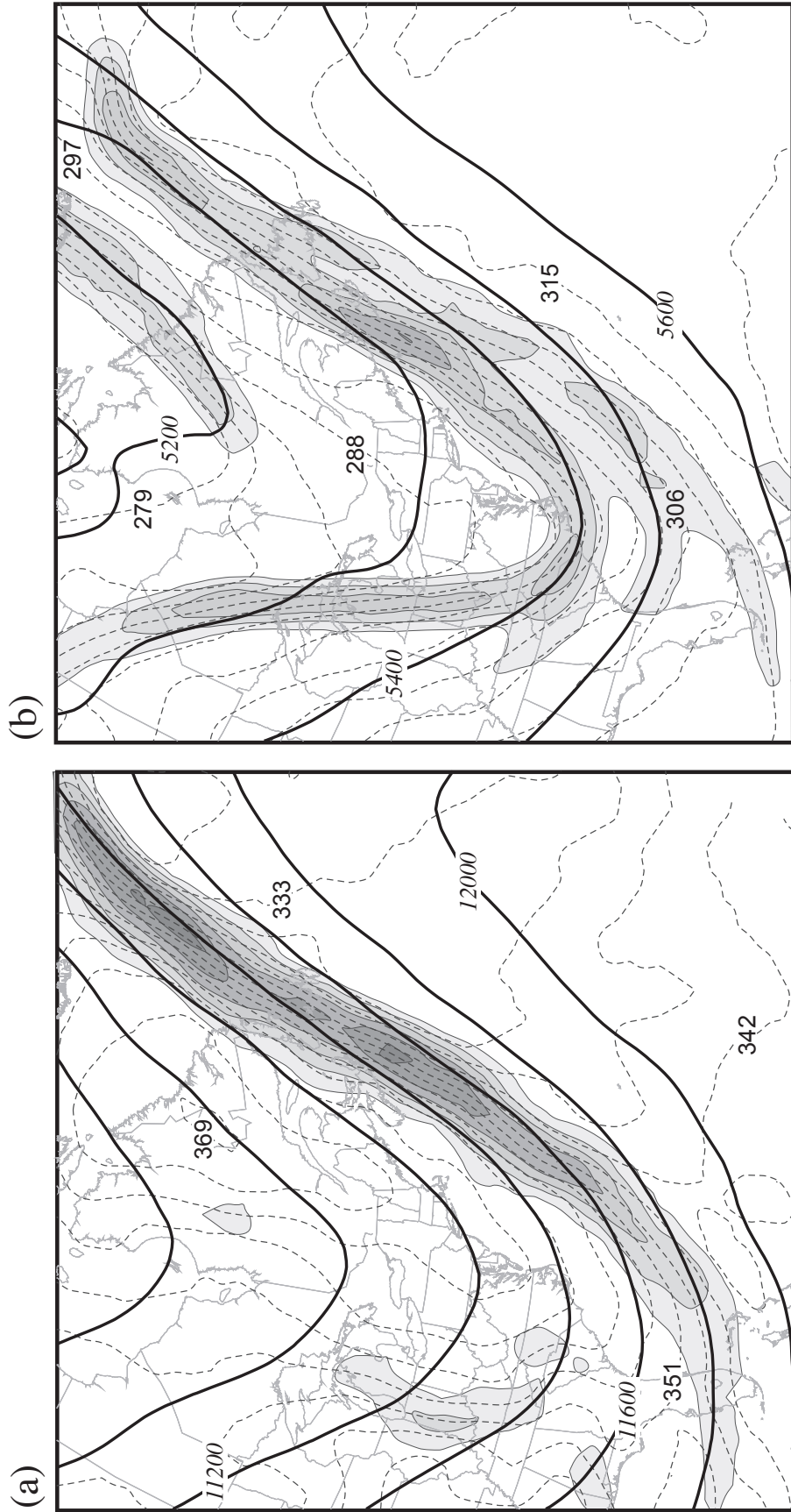


Figure 16. (a) and (b) As for Figure 5 (a) and (b), but from the Eta-104 model analysis valid at 1200 UTC 28 February 2008.

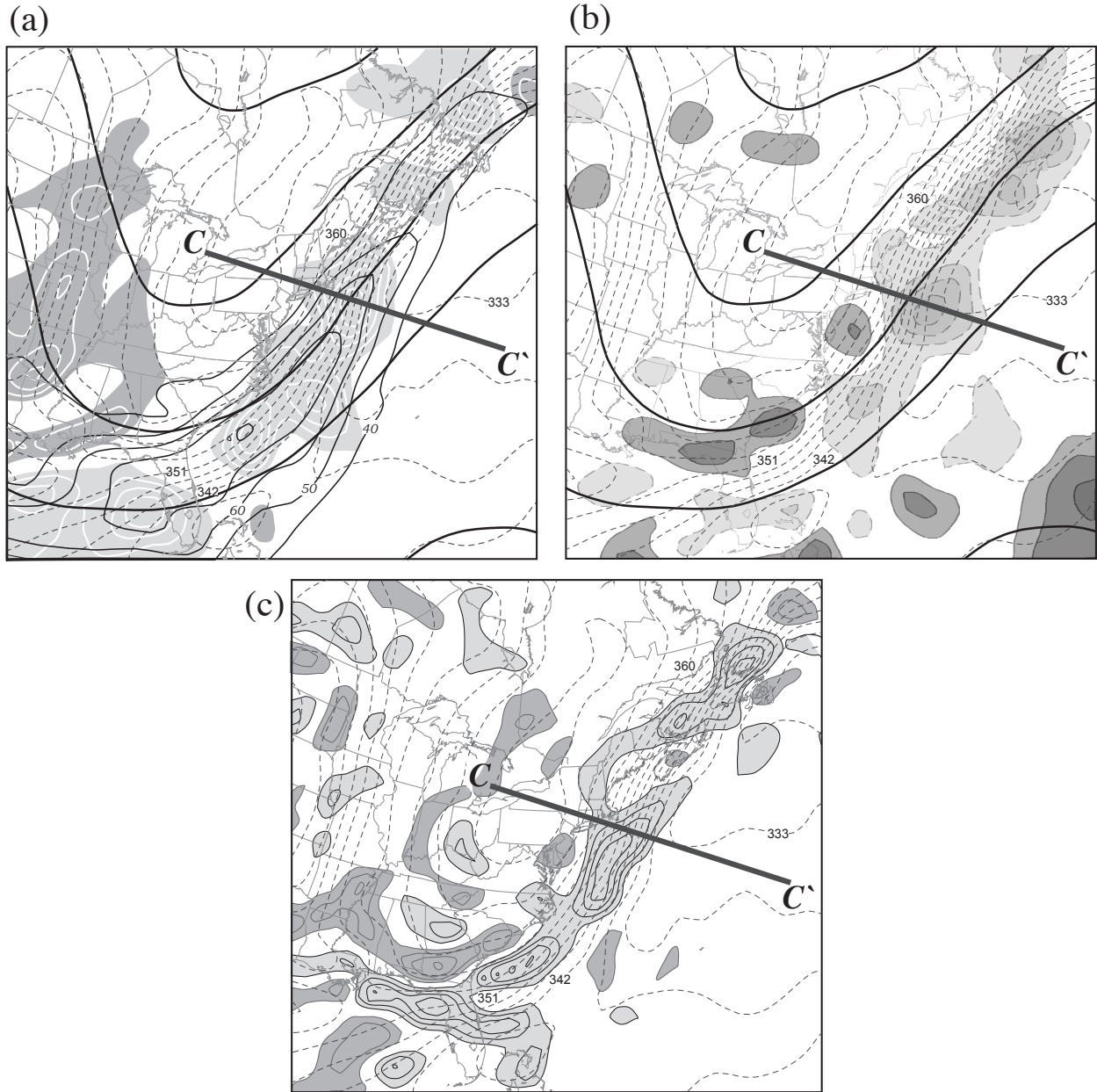


Figure 17. (a)-(c) As for Figure 9(a)-(c) but from the Eta-104 analysis valid at 0000 UTC 28 February 2008.

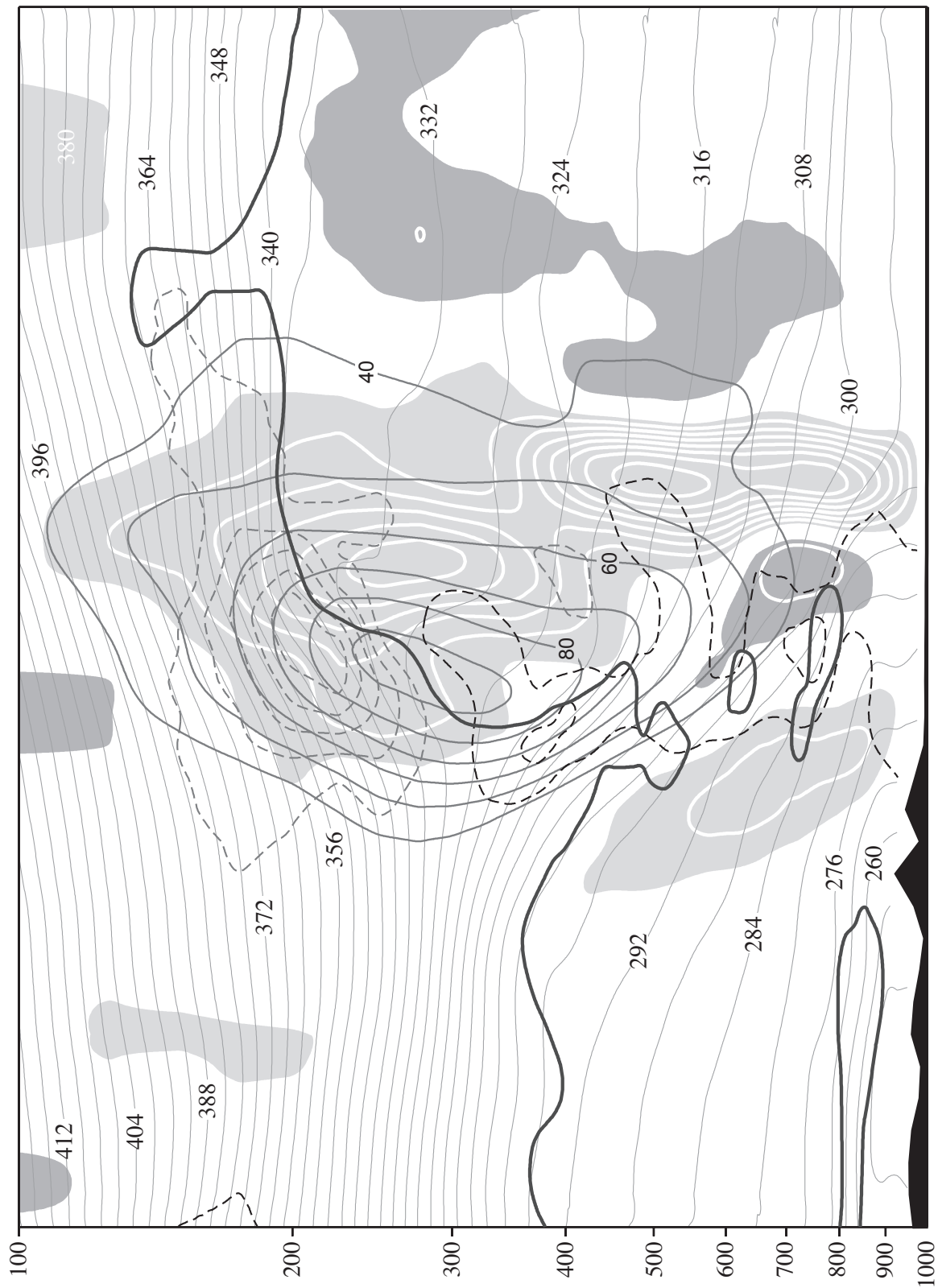


Figure 18. As for Figure 10(b), but from the Eta-104 analysis valid at 0000 UTC 28 February 2008 along the line C-C' in Figure 17(a).

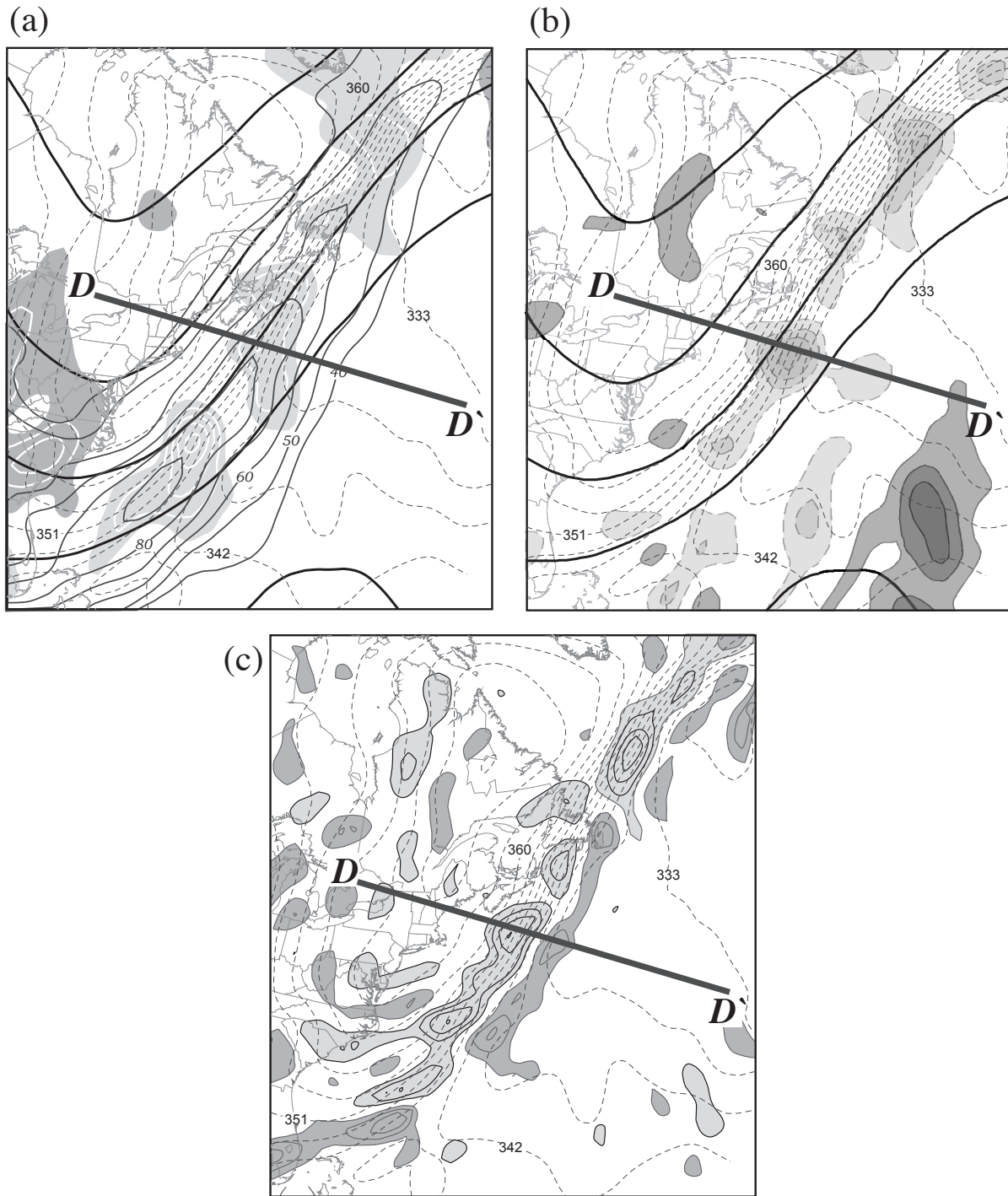


Figure 19. (a)-(c) As for Figure 9(a)-(c) but from the Eta-104 analysis valid at 1200 UTC 28 February 2008.

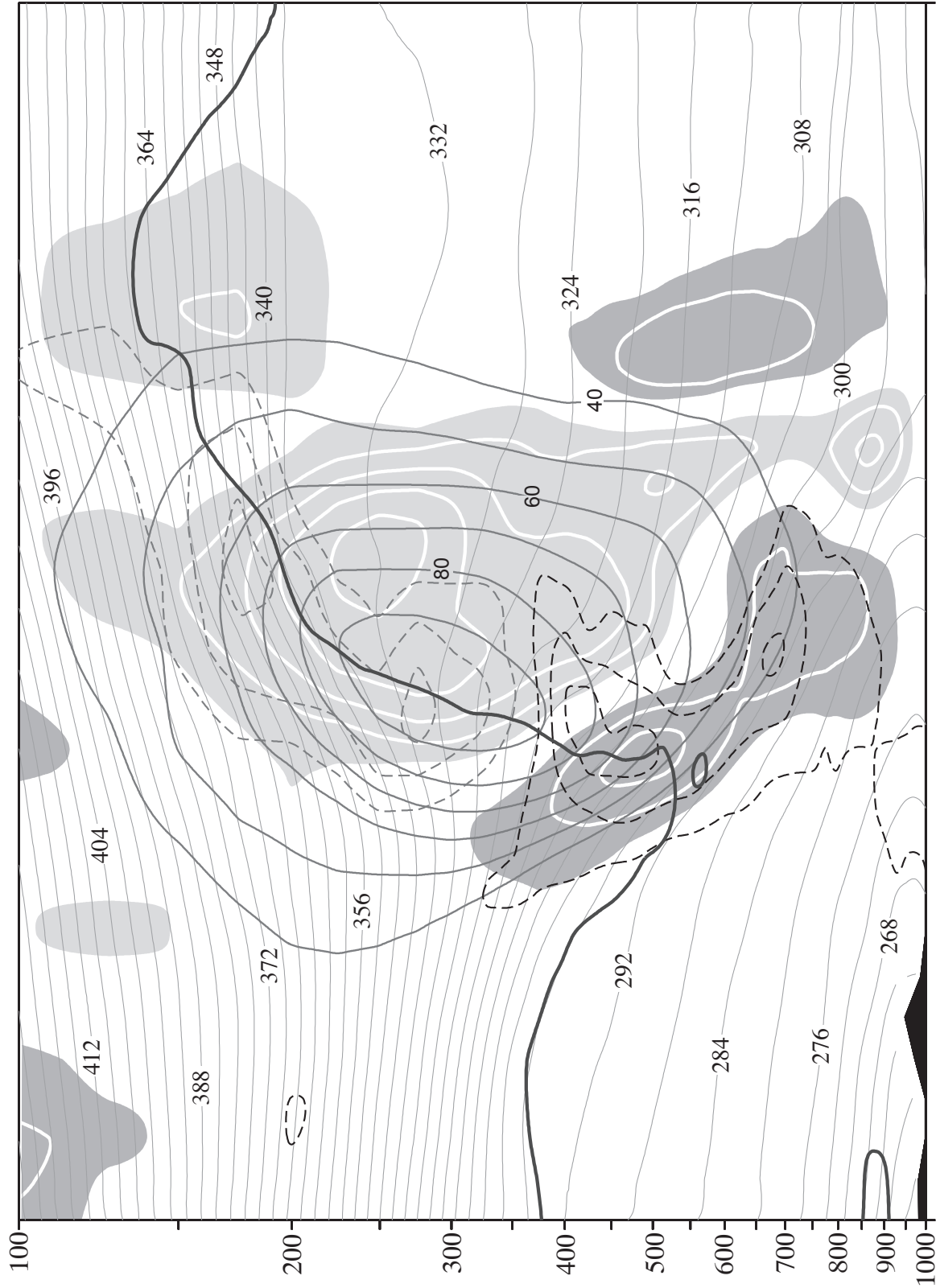


Figure 20. As for Figure 10(b), but from the Eta-104 analysis valid at 1200 UTC 28 February 2008 along the line D-D' in Figure 19(a).

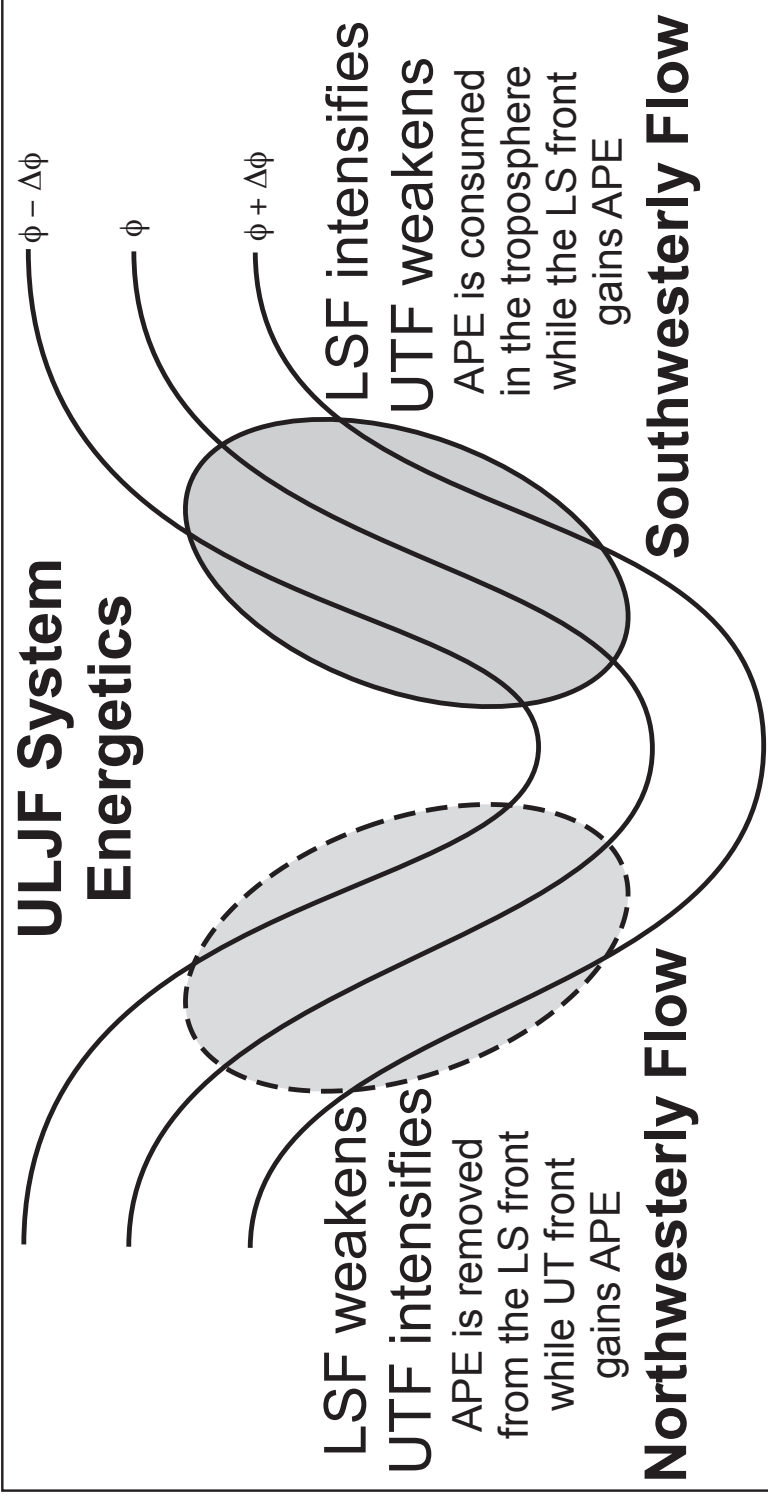


Figure 21. Schematic illustrating the asynchronous evolution of the lower stratospheric (LSF) and upper tropospheric frontal (UTF) portions of an ULJF within the northwesterly and southwesterly flow portions of a baroclinic wave. The dashed shaded oval represents the northwesterly flow region where, within an ULJF, the lower stratospheric front experiences frontolysis via vertical tilting and the upper tropospheric front experiences frontogenesis via tilting. The solid shaded oval represents the southwesterly flow region where, within an ULJF, the lower stratospheric front experiences frontogenesis via vertical tilting and the upper tropospheric front experiences frontolysis via tilting. See text for additional explanation.